administered 1-μg/ml isoproterenol solution at 1 μg·kg^{-1}·h^{-1} (Iso_1) and 10-μg/ml isoproterenol solution at 10 μg·kg^{-1}·h^{-1} (Iso_{10}) and estimated the transfer function under the control (designated as Iso_0), Iso_1, and Iso_{10} conditions.

Data analysis. The SNS command and HR were stored at a sampling rate of 200 Hz. The data were analyzed from only 2 min after the initiation of SNS to remove the initial trend of the HR increase. To estimate the transfer function from SNS to HR, we resampled the SNS-HR data pairs at 8 Hz. These data were segmented into 10 sets of half-overlapping bins of 1,024 data points each. In each segment, a linear trend was subtracted and a Hanning window was applied. The fast Fourier transform was then applied to obtain the frequency spectra of SNS and HR [9]. We calculated the ensemble averages of input power spectral density [$S_{SNS\cdot SNS}(f)$], output power spectral density [$S_{HR\cdot HR}(f)$], and cross-spectral density between the input and output [$S_{HR\cdot SNS}(f)$]. The transfer function [$H(f)$] was estimated using the following equation [10, 11].

$$H(f) = \frac{S_{HR\cdot SNS}(f)}{S_{SNS\cdot SNS}(f)} \tag{1}$$

We also calculated the magnitude-squared coherence function [$Coh(f)$] using the following equation [10, 11].

$$Coh(f) = \frac{|S_{HR\cdot SNS}(f)|^2}{S_{SNS\cdot SNS}(f)\, S_{HR\cdot HR}(f)} \tag{2}$$

The coherence function is a frequency-domain measure of the linear dependence between the input and output signals. A unity coherence value indicates a perfect linear dependence of HR on SNS, whereas a zero coherence value indicates the total independence between SNS and HR.

In *Protocols 1* and *2*, the transfer function from SNS to HR was parameterized by using a mathematical model [$H_m(f)$] of a second-order low-pass filter with pure dead time, using the following equation [3, 12].

$$H_m(f) = \frac{K}{1 + 2\zeta \frac{f}{f_N} j + \left(\frac{f}{f_N} j\right)^2} \exp(-2\pi f\, jL) \tag{3}$$

where K is the dynamic gain (in bpm/Hz), f_N is the natural frequency (in Hz), ζ is the damping ratio, and L is the pure dead time (in s); j represents the imaginary unit (see appendix B for details). A nonlinear iterative least square fitting was performed to minimize the following error function.

$$err = \frac{\sum_{i=1}^{N} |H(f_i) - H_m(f_i)|^2}{\sum_{i=1}^{N} |H(f_i)|^2}, \quad f_i = f_0 \times i \tag{4}$$

where f_0 indicates the fundamental frequency of the Fourier transform. N specifies the upper frequency bound of the fitting procedure. We set N at 32 so as to fit $H_m(f)$ to $H(f)$ up to 0.25 Hz.

In *Protocol 3*, because the transfer function from SNS to HR during Iso_{10} was significantly deviated from the mathematical model of a second-order low-pass filter with pure dead time (Eq. 3), we did not fit the mathematical model to the transfer function and adopted the transfer gain values at the lowest frequency ($G_{0.0078}$) and at 0.1 Hz ($G_{0.1}$) to represent the frequency response of HR to SNS.

Catecholamine measurements. The arterial blood sample was centrifuged and a 100-μl volume of plasma was obtained. The plasma was transferred into a 1.5-ml polypropylene conical tube. A 50-μl volume of the working internal standard solution [100 pg of 3,4-dihydroxybenzylamine (DHBA)], 5 mg of acid-washed alumina, and 1.0 ml of 1-M tris(hydroxymethyl) aminomethane buffer (pH 8.6), containing 0.2% disodium ethylendiaminetetraacetic acid (EDTA), was added to the conical tube and shaken for 15 min. After shaking, the alumina was washed three times with distilled water, transferred into a microfilter (Ultrafree C3, Millipore, Bedford, MA), and centrifuged to remove excess fluid. NA, Adr, and DHBA were then eluted from the alumina, using 60 μl of 2% acetic acid, and their concentrations were measured by using high-performance liquid chromatography with electrochemical detection (DTA-300, Eicom, Kyoto, Japan). Plasma NA and Adr concentrations were calculated, taking into account the recovery rate of DHBA.

Statistical analysis. All data are presented in mean and mean ± SEM values. In *Protocol 1*, the effect of dynamic SNS on the plasma NA concentration was examined by a paired t-test under NA_0 condition. The NA and Adr concentrations before SNS were compared among NA_0, NA_1, and NA_{10} conditions, using Dunnett's test against a single control following the repeated-measures analysis of variance [13]. We also compared mean HR, mean AP, and parameters of the transfer function among NA_0, NA_1, and NA_{10} conditions, using Dunnett's test following repeated-measures analysis of variance. In *Protocol 2*, the effect of dynamic SNS on the plasma Adr concentration was examined by a paired t-test under Adr_0 condition. Other values, including plasma NA and Adr concentrations, mean HR, mean AP, and parameters of the transfer function, were compared among Adr_0, Adr_1, and Adr_{10} conditions, using Dunnett's test following repeated-measures analysis of variance. In *Protocol 3*, mean HR, mean AP, and gain values ($G_{0.0078}$ and $G_{0.1}$) were compared among Iso_0, Iso_1,

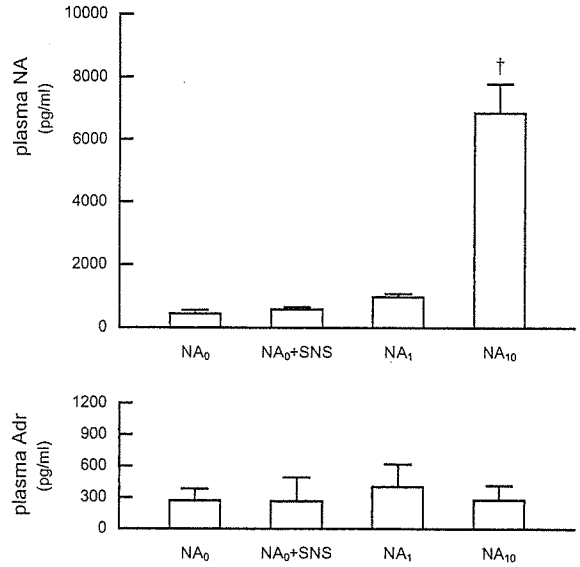

Fig. 2. Plasma concentrations of NA and Adr obtained from *Protocol 1*. The plasma NA concentration was significantly increased during the NA_{10} condition. The plasma Adr concentration was not changed significantly by the NA infusion. NA_0: saline infusion; NA_1 and NA_{10}: noradrenaline infusions at 1 and 10 $\mu g \cdot kg^{-1} \cdot h^{-1}$.

and Iso_{10} conditions, using Dunnett's test following repeated-measures analysis of variance. In all of the statistics, the difference was considered significant at $P < 0.05$.

RESULTS

Effects of high plasma NA on the dynamic sympathetic neural regulation of HR

In *Protocol 1*, dynamic SNS for 15 min did not change the plasma NA or Adr concentration significantly during NA_0 condition (Fig. 2, NA_0 vs. NA_0+SNS). The plasma NA concentration prior to dynamic SNS did not increase significantly during NA_1 condition, but increased to approximately 15 times higher during NA_{10} condition compared to NA_0 condition. The NA infusion did not significantly affect the plasma Adr concentration.

Figure 3A illustrates the time series of SNS, HR, and AP under NA_0, NA_1, and NA_{10} conditions obtained from one animal. The SNS was assigned at 0 or 5 Hz according to a binary white noise sequence. HR changed randomly in response to the dynamic SNS. Mean HR was slightly increased during NA infusion, whereas the amplitude of HR variation appeared unchanged. Mean AP was increased during NA_{10} condition compared to NA_0 condition.

Figure 3B shows averaged transfer functions from SNS to HR during NA_0, NA_1, and NA_{10} conditions obtained from all six animals in *Protocol 1*. The solid curve and the dashed curves in each plot represent mean and mean ± SEM values, respectively. In the gain plot, the transfer

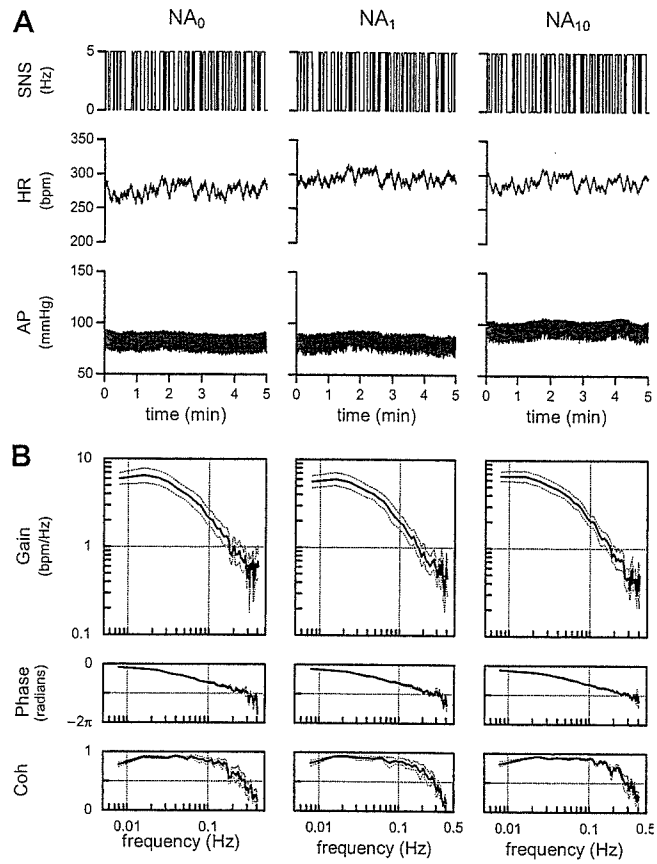

Fig. 3. A: Time series of one animal obtained from *Protocol 1*. Sympathetic nerve stimulation (SNS), heart rate (HR), and arterial pressure (AP) are shown. HR changed dynamically in response to SNS. **B**: Averaged transfer functions from SNS to HR during NA_0, NA_1, and NA_{10} conditions obtained from *Protocol 1* (n = 6). NA infusion did not affect the transfer function significantly except for changes in the damping ratio. Solid and dashed curves indicate mean and mean ± SEM values, respectively.

gain decreased with increasing frequency, reflecting the low-pass characteristics of the sympathetic neural regulation of HR. In the phase plot, the phase was near zero radians at the lowest frequency and delayed with increasing frequency, reflecting the SNS increases of HR. In the coherence plot, high coherence values up to 0.2 Hz indicate that approximately 80% of the HR variation in this frequency range was explained by the linear dynamics between SNS and HR. The transfer functions were similar among the three conditions. The dynamic gain, natural frequency, and pure dead time did not differ among the three conditions (Table 1). However, the damping ratio was significantly greater during NA_1 and NA_{10} conditions compared to the NA_0 condition.

Mean HR before SNS did not differ among NA_0, NA_1, and NA_{10} conditions, whereas mean HR during SNS increased significantly during NA_1 and NA_{10} conditions compared to NA_0 condition (Table 1). Although the repeated-measures analysis of variance indicated that the ef-

Table 1. Parameters obtained from *Protocol 1*.

	NA_0	NA_1	NA_{10}
HR, bpm			
Before SNS	248 ± 20	250 ± 19	251 ± 20
During SNS	280 ± 24	289 ± 22**	288 ± 22**
AP, mmHg			
Before SNS	95.7 ± 7.2	99.3 ± 8.1	106.6 ± 6.6*
During SNS	93.6 ± 8.0	102.9 ± 8.8**	106.0 ± 7.0**
Dynamic gain (K), bpm/Hz	7.6 ± 1.2	7.5 ± 1.1	8.1 ± 1.1
Natural frequency (f_N), Hz	0.080 ± 0.010	0.084 ± 0.010	0.083 ± 0.010
Damping ratio (ζ)	1.16 ± 0.05	1.48 ± 0.03*	1.52 ± 0.11*
Pure dead time (L), s	0.44 ± 0.08	0.55 ± 0.07	0.52 ± 0.06
Fitting error (err), %	1.6 ± 0.3	2.2 ± 0.6	1.6 ± 0.4

Values are means ± SEM. $^{**}P < 0.01$ and $^{*}P < 0.05$ vs. the corresponding value obtained during NA_0 condition. HR: heart rate. AP: arterial pressure. SNS: sympathetic nerve stimulation.

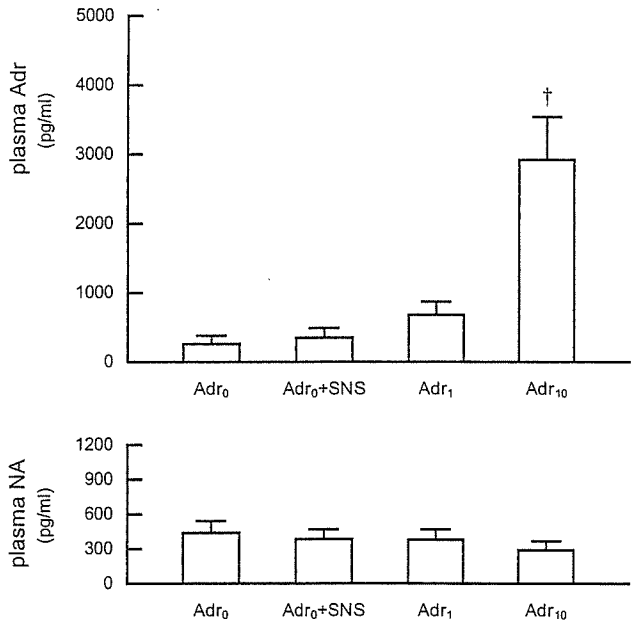

Fig. 4. Plasma concentrations of Adr and NA obtained from *Protocol 2*. The plasma Adr concentration was significantly increased during the Adr_{10} condition. The plasma NA concentration was not changed significantly by Adr infusion. Adr_0: saline infusion; Adr_1 and Adr_{10}: adrenaline infusions at 1 and 10 μg·kg^{-1}·h^{-1}.

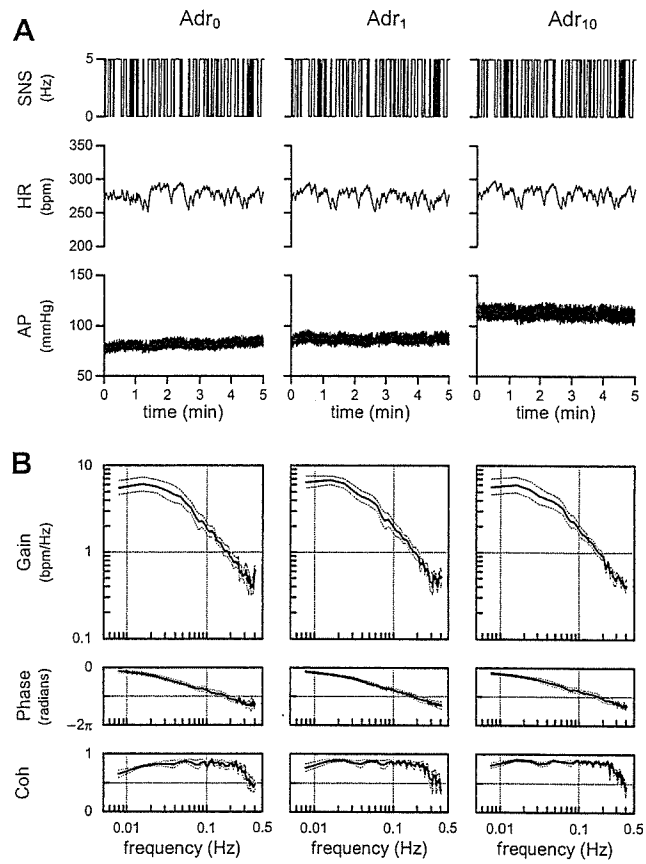

Fig. 5. A: Time series of one animal obtained from *Protocol 2*. HR changed dynamically in response to SNS. **B**: Averaged transfer functions from SNS to HR during Adr_0, Adr_1, and Adr_{10} conditions obtained from *Protocol 2* ($n = 6$). Adr infusion did not affect the transfer function significantly. Solid and dashed curves indicate mean and mean ± SEM values, respectively.

fects of NA infusion on mean HR during SNS were significant, the magnitude of the HR increase was small relative to the interindividual variation of HR. Mean AP before SNS was significantly elevated during NA_{10} condition, but not during NA_1 condition compared to NA_0 condition. Mean AP during SNS was increased significantly during both NA_1 and NA_{10} conditions compared to NA_0 condition.

Table 2. Parameters obtained from *Protocol 2*.

	Adr_0	Adr_1	Adr_{10}
HR, bpm			
Before SNS	231 ± 12	232 ± 10	228 ± 7
During SNS	274 ± 13	275 ± 13	274 ± 13
AP, mmHg			
Before SNS	93.1 ± 9.7	99.0 ± 8.3	113.7 ± 5.2**
During SNS	101.3 ± 8.0	103.8 ± 8.4	116.6 ± 4.6**
Dynamic gain (K), bpm/Hz	8.0 ± 0.6	8.4 ± 0.8	8.2 ± 1.0
Natural frequency (f_N), Hz	0.070 ± 0.005	0.071 ± 0.005	0.067 ± 0.006
Damping ratio (ζ)	1.09 ± 0.20	1.32 ± 0.11	1.39 ± 0.17
Pure dead time (L), s	0.55 ± 0.13	0.66 ± 0.09	0.63 ± 0.15
Fitting error (err), %	2.5 ± 0.5	1.8 ± 0.3	2.3 ± 0.6

Values are means ± SEM. **$P < 0.01$ vs. the corresponding value obtained during Adr_0 condition. HR: heart rate. AP: arterial pressure. SNS: sympathetic nerve stimulation.

Effects of high plasma Adr on the dynamic sympathetic neural regulation of HR

In *Protocol 2*, dynamic SNS for 15 min did not significantly change the plasma Adr or NA concentration during Adr_0 condition (Fig. 4, Adr_0 vs. Adr_0+SNS). The plasma Adr concentration prior to dynamic SNS did not increase significantly during Adr_1 condition, but increased to approximately 11 times higher during Adr_{10} condition compared to Adr_0 condition. The Adr infusion did not significantly affect the plasma NA concentration.

Figure 5A illustrates the time series of SNS, HR, and AP during Adr_0, Adr_1, and Adr_{10} conditions obtained from one animal. HR changed randomly in response to the dynamic SNS. The Adr infusion did not significantly change mean HR or the amplitude of HR variation among Adr_0, Adr_1, and Adr_{10} conditions. Mean AP increased during Adr_{10} condition compared to the Adr_0 condition.

Figure 5B shows averaged transfer functions from SNS to HR during Adr_0, Adr_1, and Adr_{10} conditions obtained from all of the six animals in *Protocol 2*. There seem to be no effects of Adr infusion on the transfer functions. No significant differences in dynamic gain, natural frequency, damping ratio, and pure dead time were observed among the three conditions (Table 2).

Mean HR did not differ significantly among Adr_0, Adr_1, and Adr_{10} conditions, both before and during SNS (Table 2). Mean AP increased significantly during Adr_{10} condition, but not during Adr_1 condition compared with Adr_0 condition, both before and during SNS.

Effects of intravenous isoproterenol on the dynamic sympathetic neural regulation of HR

Figure 6A illustrates the time series of SNS, HR, and AP during Iso_0, Iso_1, and Iso_{10} conditions obtained from one animal. HR changed randomly in response to the dynamic SNS under the Iso_0 condition. Although the dynamic HR response to SNS was maintained under the Iso_1 condition, mean HR was significantly elevated, and no apparent HR response was observed under the Iso_{10} condition.

Figure 6B shows averaged transfer functions from SNS to HR during Iso_0, Iso_1, and Iso_{10} conditions obtained from all of the six animals in *Protocol 3*. The transfer function showed a slight downward shift under the Iso_1 condition compared to the Iso_0 condition. It was significantly deformed and lost consistent characteristics across the animals under the Iso_{10} condition, as evidenced by large standard errors (dashed lines). The gain values ($G_{0.0078}$ and $G_{0.1}$) were significantly lower under the Iso_{10} condition compared to the Iso_0 condition (Table 3).

Mean HR did not change significantly under the Iso_1 condition, but increased significantly under the Iso_{10} condition compared to that under the Iso_0 condition, both before and during SNS (Table 3). Mean AP before SNS was significantly increased under the Iso_1 condition, but not under the Iso_{10} condition compared to that under the Iso_0 condition. Mean AP during SNS did not differ under the Iso_1 condition, but decreased significantly under the Iso_{10} condition compared to that under the Iso_0 condition.

DISCUSSION

We have examined the effects of high plasma NA or Adr on the transfer function from SNS to HR and found that high plasma catecholamines within physiological limits (approximately 10 times the resting levels) were ineffective to alter the sympathetic neural regulation of HR. Although the baseline HR was higher than the resting HR reported in conscious rabbits, the high baseline HR may be partly due to vagotomy. Because dynamic SNS (average stimulation frequency was 2.5 Hz) could increase mean HR, on the average, by 32 bpm in *Protocol 1* and by 43 bpm in *Protocol 2* under control conditions (NA_0 and Adr_0), the insignificant effects of high plasma catecholamines on HR cannot be explained by a simple saturation

Table 3. Parameters obtained from *Protocol 3*.

	Iso_0	Iso_1	Iso_{10}
HR, bpm			
Before SNS	244 ± 7	245 ± 6	289 ± 8**
During SNS	278 ± 11	280 ± 10	293 ± 9**
AP, mmHg			
Before SNS	80.2 ± 8.5	96.2 ± 4.9*	83.5 ± 7.1
During SNS	90.9 ± 7.4	93.1 ± 7.4	82.9 ± 7.0**
$G_{0.0078}$, bpm/Hz	5.9 ± 1.0	4.7 ± 0.8	1.0 ± 0.4**
$G_{0.1}$, bpm/Hz	1.3 ± 0.3	0.9 ± 0.2	0.2 ± 0.2**

Values are means ± SEM. $^{**}P < 0.01$ and $^{*}P < 0.05$ vs. the corresponding value obtained during Iso_0 condition. HR: heart rate. AP: arterial pressure. SNS: sympathetic nerve stimulation. $G_{0.0078}$: transfer gain value at 0.0078 Hz. $G_{0.1}$: transfer gain value at 0.1 Hz.

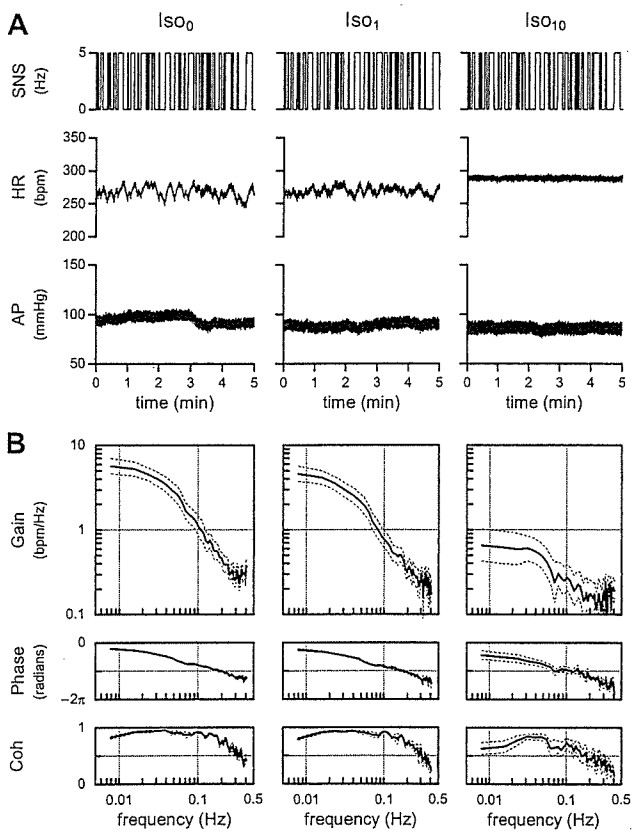

Fig. 6. A: Time series of one animal obtained from *Protocol 3*. Although HR changed dynamically in response to SNS under Iso_0 and Iso_1 conditions, mean HR elevated significantly, and no apparent dynamic HR response was observed under the Iso_{10} condition. **B**: Averaged transfer functions from SNS to HR during Iso_0, Iso_1, and Iso_{10} conditions obtained from *Protocol 3* (n = 6). The transfer gain reduced significantly and varied among animals, as evidenced by the large SEM under the Iso_{10} condition. Solid and dashed curves indicate mean and mean ± SEM values, respectively. Iso_0: saline infusion; Iso_1 and Iso_{10}: isoproterenol infusions at 1 and 10 μg·kg^{-1}·h^{-1}.

phenomenon of the HR response to catecholamines or by complete downregulation of β-adrenergic receptors under the present experimental settings. Actually, we confirmed that the same dose of intravenous administration of a β-adrenergic agonist isoproterenol increased mean HR significantly and blunted the transfer function (Fig. 6, Iso_{10} in *Protocol 3*). It is quite likely that NA released from the sympathetic nerve terminals during SNS has much stronger effects on HR in comparison with circulating catecholamines.

Effects of high plasma NA on the sympathetic neural regulation of HR

The plasma NA concentration increased approximately 15 times higher during NA_{10} condition than during NA_0 condition. Nevertheless, mean HR before SNS did not change significantly during NA_{10} condition compared to NA_0 condition (Table 1). In contrast, mean AP before SNS increased significantly during NA_{10} condition compared to NA_0 condition (Table 1). Young *et al.* [14] also reported an increase in AP and no changes in HR during NA infusion at 0.2 μg·kg^{-1}·min^{-1} (12 μg·kg^{-1}·h^{-1}) in conscious dogs, though the baroreflexes could have counteracted the potential increase of HR in their study. These results indicate that the vascular bed is more responsive to plasma NA than the sinus node. A tighter synaptic cleft of the neuroeffector junction of the cardiac muscle compared to the vasculature, though it was reported in rat tissues [15], might explain the differential sensitivity to plasma NA between HR and AP.

Cardiac SNS significantly increased the mean HR without increasing the plasma NA concentration (Fig. 2), consistent with previous studies in anesthetized dogs [16] and cats [17]. Although mean HR before SNS did not differ among NA_0, NA_1, and NA_{10} conditions, mean HR during SNS was significantly higher during NA_1 and NA_{10} conditions compared to control (Table 1). These results are in opposition to the hypothesis that high plasma NA activates presynaptic α_2-adrenergic receptors and attenuates the HR response to SNS. One possible explanation for the increased mean HR during SNS under conditions of the NA infusion is as follows. NA released from the sympathetic nerve terminals is removed from the synaptic cleft by two catecholamine uptake mechanisms: a high-affinity, low-capacity neuronal uptake ($uptake_1$) and a low-affinity, high-capacity extraneuronal uptake ($uptake_2$) [5,

18, 19]. The uptake$_1$ mechanism also contributes to plasma clearance of NA [20]. High plasma NA might occupy the uptake$_1$ process to some extent and slow the NA removal from the synaptic cleft during SNS. As a result, the positive chronotropic effects of SNS might be augmented. Honda *et al.* [8] investigated the relationship between the kinetics of plasma catecholamines and cardiac sympathetic nerve activity during systemic hypotension induced by vena cava occlusion. They showed that the cardiac uptake of NA proportionally increased as the arterial NA concentration increased and that there was a negative correlation between the cardiac uptake of NA and the percent increase in mean cardiac sympathetic nerve activity. The negative correlation between the cardiac uptake of NA and the percent increase in mean cardiac sympathetic nerve activity might support the notion that NA of plasma origin and that of neural origin share the uptake$_1$ process. Although the within-individual change was statistically significant, the magnitude of HR increase during SNS was small compared to the interindividual variation of mean HR. Therefore the augmentation of the positive chronotropic effects by high plasma NA may be physiologically insignificant.

In the transfer function parameters, the damping ratio alone was significantly increased during NA_1 and NA_{10} conditions compared with NA_0 condition (Table 1). As already discussed, high plasma NA might have interfered with the uptake$_1$ process and consequently changed the damping ratio of the transfer function [12]. The damping ratio is an important determinant of the system behavior of the second-order low-pass filter. Depending on the value of the damping ratio, the system behaves as underdamped ($0 < \zeta < 1$), critically damped ($\zeta = 1$), or overdamped ($\zeta > 1$) (see appendix B). In the present study, however, the damping ratios changed only from 1.2 to 1.5; thus the system should behave as over-damped under any of the NA_0, NA_1, and NA_{10} conditions. Given that other transfer function parameters including the dynamic gain, natural frequency, and pure dead time did not change significantly, high plasma NA has limited effects on the transfer function from SNS to HR.

Effects of high plasma Adr on the sympathetic neural regulation of HR

The plasma Adr concentration during Adr_{10} condition increased to approximately 11 times that during Adr_0 condition. Although high plasma Adr did not increase HR, it did increase AP (Table 2). In contrast, Young *et al.* [14] reported that an administration of Adr at 0.2 $\mu g \cdot kg^{-1} \cdot min^{-1}$ (12 $\mu g \cdot kg^{-1} \cdot h^{-1}$) significantly increased both AP and HR in conscious dogs. Since the plasma Adr concentration in their study increased to a similar degree to the present result, the HR response to plasma Adr may differ between rabbits and dogs. Other factors that potentially explain the discrepancy are the vagotomy and anesthesia used in the present study. On the other hand, the Adr administration could have altered cardiac sympathetic neural outflow in the study by Young *et al.* [14].

In the present experimental conditions, high plasma Adr did not increase mean HR during SNS compared to Adr_0 condition and did not affect the transfer function from SNS to HR either (Table 2). These results are in opposition to the hypothesis that high plasma Adr activates presynaptic β_2-adrenergic receptors and augments the HR response to SNS. Moreover, because Adr has lower affinity to the uptake$_1$ process compared to NA [18, 19], high plasma NA but not Adr affected the mean HR during SNS and the damping ratio of the transfer function via the mechanism of modulating the NA removal.

The present results are consistent with the study of Boudreau *et al.* [21], in which a 10-min administration of Adr (92 $ng \cdot kg^{-1} \cdot min^{-1}$ or 5.5 $\mu g \cdot kg^{-1} \cdot h^{-1}$) did not increase the NA release in response to cardiac SNS in anesthetized dogs. However, Boudreau *et al.* [21] also demonstrated that a 180-min administration of Adr did increase the NA release in response to cardiac SNS, along with an increased Adr level in the cardiac tissue. Plasma Adr can be taken up into the sympathetic nerve terminals and then coreleased with NA [22]. When Adr is coreleased with NA into the synaptic cleft, NA release may be facilitated via the presynaptic β_2-adrenergic mechanism because Adr is a more potent agonist for β_2-adrenergic receptors than NA [23]. Although the long-term effects of high plasma Adr on the transfer function from SNS to HR was not examined in the present study, it is conceivable that high plasma Adr does not affect the sympathetic neural regulation of HR unless the Adr accumulation in the sympathetic nerve terminals reaches a concentration that is high enough.

Effects of intravenous isoproterenol on the dynamic sympathetic neural regulation of HR

As expected, an intravenous administration of isoproterenol at 10 $\mu g \cdot kg^{-1} \cdot h^{-1}$ increased mean HR significantly both before and during SNS. The transfer gain of the HR response to SNS was significantly decreased under the Iso_{10} condition (Table 3). These results are similar to our previous finding that an increase in mean stimulation frequency of SNS increased mean HR and decreased the transfer gain [12]. We have explained a bidirectional augmentation of the dynamic HR response to autonomic nerve stimulation by using a nonlinear sigmoidal relationship between the autonomic tone and HR [3, 24]. In that concept, the operating point of HR critically affects the transfer gain of the HR response to sympathetic or vagal nerve stimulation; i.e., deviation of the operating point from the center of the sigmoidal relationship decreases the tangential line of the sigmoid curve that relates to the transfer gain. Such operating-point dependence of the transfer gain may explain, at least in part, the decrease in

the transfer gain under the Iso_{10} condition.

Several limitations need to be addressed. First, we performed the experiment in anesthetized rabbits. Because the anesthesia would affect the autonomic tone, the results may not be directly applicable to conscious animals. However, because we cut and stimulated the right cardiac sympathetic nerve, changes in autonomic outflow associated with anesthesia might not have significantly affected the present results. Second, as already mentioned, species differences in HR response to catecholamines may exist. Whether high plasma catecholamines affect the dynamic sympathetic neural regulation of HR in animal species other than rabbits requires further investigations. Third, the duration of catecholamine administration prior to SNS was set at 15 min. Although this priming time was sufficient for AP and HR to reach new steady states, the effects of longer durations of high plasma catecholamines on the dynamic sympathetic neural regulation of HR remain to be investigated. And fourth, because we stimulated the cardiac postganglionic sympathetic nerve, the possible effects of high plasma catecholamines on sympathetic ganglionic transmission were excluded.

In conclusion, although plasma NA or Adr were increased to a level 10–15 times higher than the baseline level by exogenous administration, such high plasma NA or Adr did not significantly affect the dynamic sympathetic neural regulation of HR in anesthetized rabbits. Although humoral and neural factors are thought to regulate the cardiovascular system in concert, the neural factor appears to be much stronger than the humoral factor as far as the HR regulation is concerned.

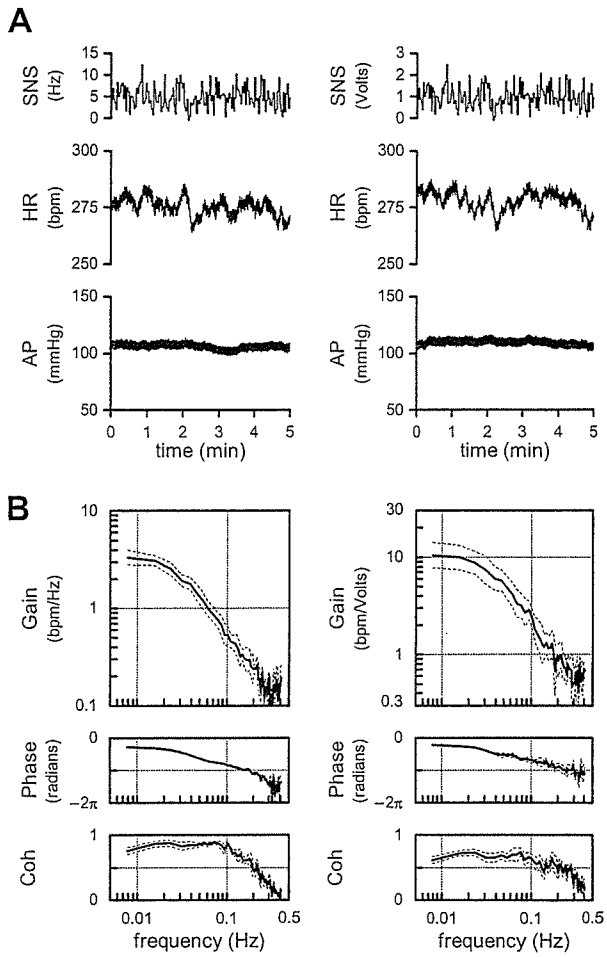

Fig. 7. A: Time series of SNS, HR, and AP using frequency modulation (left) and amplitude modulation (right) as the input signal. HR changed dynamically in response to both the frequency modulation and amplitude modulation of SNS. **B**: Averaged transfer functions obtained from 5 animals using frequency modulation (left) and amplitude modulation (right) as the input signal. Although the absolute gain values are different because of different units in inputs, the low-pass characteristics are in common for both transfer functions.

APPENDIX A

Frequency modulation versus amplitude modulation in nerve stimulation. Because the sinus node responds to NA released from the sympathetic nerve terminals and because the NA kinetics at the neuroeffector junction predominantly determine the low-pass filter characteristics of the HR response to SNS [12], whether the SNS is modulated by frequency or amplitude will not significantly affect the transfer function from SNS to HR. Although the frequency modulation and the amplitude modulation would reveal different nonlinear input-output relationships between the stimulation command signal and the number of nerve fibers actually discharged, a transfer function analysis using a white noise input can retrieve a linear input-output relationship even in the presence of a significant nonlinearity [11]. Although the SNS we used is different from a physiological discharge of nerve fibers, the HR response to physiological nerve discharge would obey the same principle characterized by the transfer function from SNS to HR. When we estimated the transfer function from recorded sympathetic nerve activity to HR, it also approximates to the second-order low-pass filter with pure dead time [25].

We compared the transfer function from SNS to HR identified by the frequency-modulation input and that by the amplitude-modulation input in 5 anesthetized rabbits. The left panel of Fig. 7A shows a typical time series of SNS, HR, and AP obtained from the frequency-modulation input with a constant amplitude of 3 V (2-ms pulse width, 2-s switching interval). The right panel of Fig. 7A shows the time series obtained from the amplitude-modulation input with a constant frequency of 5 Hz (2-ms pulse width, 2-s switching interval). Figure 7B summarizes the averaged transfer function obtained by the frequency-modulation input (left panel) and that by the amplitude-modulation input (right panel). Although the units of gain differ between the two, general low-pass characteristics were in common. The coherence values associated with

the amplitude-modulation input seems smaller than those associated with the frequency-modulation input. In regard to the amplitude-modulation input, the stimulation amplitude usually crosses the threshold amplitude, below which the nerve fibers do not discharge. Such a nonlinear process of the amplitude-modulation input would contribute to the lower coherence values.

APPENDIX B

A mathematical modeling of dynamic heart rate response to sympathetic nerve stimulation using a second-order low-pass filter with pure dead time. We adopted a mathematical model of a second-order low-pass filter with pure dead time to quantify the transfer function from SNS to HR. In the left panel of Fig. 8, the thick line represents a typical transfer function obtained under the NA_0 condition in one animal. The thin smooth curve represents a best-fit mathematical model. A schematic explanation of the model parameters is shown in the right panel of Fig. 8. The dynamic gain, K, determines the value the transfer gain approaches as the frequency goes to zero. The natural frequency, f_N, determines the frequency of low-pass characteristics. The phase of the second-order low-pass filter delays by $\pi/2$ radians at f_N when the pure dead time is zero. The damping ratio, ζ, determines how fast the transfer gain wanes around f_N. As an example, the gain plot shows a slight peaking around f_N when $\zeta = 0.5$. On the other hand, the gain plot shows a more gradual decrease around f_N when $\zeta = 2.0$. The maximum phase delay of the second-order low-pass filter is π radians. The pure dead time, L, determines the additional phase delay necessary for explaining the phase difference between the measured transfer function and the second-order low-pass filter.

This study was supported by "Health and Labour Sciences Research Grant for Research on Advanced Medical Technology" from the Ministry of Health, Labour and Welfare of Japan; "Health and Labour Sciences Research Grant for Research on Medical Devices for Analyzing, Supporting and Substituting the Function of Human Body" from the Ministry of Health, Labour and Welfare of Japan; "Health and Labour Sciences Research Grant H18-Iryo-Ippan-023" from the Ministry of Health, Labour and Welfare of Japan; "Program for Promotion of Fundamental Studies in Health Science" from the National Institute of Biomedical Innovation, a grant provided by the Ichiro Kanehara Foundation; "Ground-based Research Announcement for Space Utilization" promoted by the Japan Space Forum; and "Industrial Technology Research Grant Program in 03A47075" from the New Energy and Industrial Technology Development Organization (NEDO) of Japan.

REFERENCES

1. Kawada T, Fujiki N, Hosomi H. Systems analysis of the carotid sinus baroreflex system using a sum-of-sinusoidal input. Jpn J Physiol. 1992;42:15-34.
2. Kawada T, Yamamoto K, Kamiya A, Ariumi H, Michikami D, Shishido T, Sunagawa K, Sugimachi M. Dynamic characteristics of carotid sinus pressure-nerve activity transduction in rabbits. Jpn J Physiol. 2005;55:157-63.
3. Kawada T, Ikeda Y, Sugimachi M, Shishido T, Kawaguchi O, Yamazaki T, Alexander J Jr, Sunagawa K. Bidirectional augmentation of heart rate regulation by autonomic nervous system in rabbits. Am J Physiol Heart Circ Physiol. 1996;271:H288-95.
4. Kawada T, Sugimachi M, Shishido T, Miyano H, Ikeda Y, Yoshimura R, Sato T, Takaki H, Alexander J Jr, Sunagawa K. Dynamic vagosympathetic interaction augments heart rate response irrespective of stimulation patterns. Am J Physiol Heart Circ Physiol. 1997;272:H2180-7.
5. Cryer PE. Physiology and pathophysiology of the human sympathoadrenal neuroendocrine system. N Eng J Med. 1980;303:436-44.
6. Langer SZ, Adler-Graschinsky E, Giorgi O. Physiological significance of α-adrenoceptor-mediated negative feedback mechanism regulating noradrenaline release during nerve stimulation. Nature. 1977;265:648-50.
7. Majewski H, Rand MJ, Tung LH. Activation of prejunctional β-adrenoceptors in rat atria by adrenaline applied exogenously or released as a co-transmitter. Br J Pharmacol. 1981;73:669-79.
8. Honda T, Ninomiya I, Azumi T. Cardiac sympathetic nerve activity and catecholamine kinetics in cat hearts. Am J Pysiol Heart Circ Physiol. 1987;252:H879-85.
9. Brigham EO. The Fast Fourier Transform and Its Applications. Englewood Cliffs, NJ: Prentice-Hall; 1988. p. 167-203.
10. Bendat JS, Piersol AG. Random Data Analysis and Measurement Procedures. 3rd ed. New York: John Wiley & Sons; 2000. p. 189-217.
11. Marmarelis PZ, Marmarelis VZ. Analysis of Physiological Systems. New York: Plenum; 1978. p. 131-221.
12. Nakahara T, Kawada T, Sugimachi M, Miyano H, Sato T, Shishido T, Yoshimura R, Miyashita H, Inagaki M, Alexander J Jr, Sunagawa K. Neuronal uptake affects dynamic characteristics of heart rate response to sympathetic stimulation. Am J Physiol Regul Integr Comp Physiol. 1999;277:R140-6.
13. Glantz SA. Primer of Biostatistics (5th ed). New York: McGraw-Hill; 2002.
14. Young MA, Hintze TH, Vatner SF. Correlation between cardiac performance and

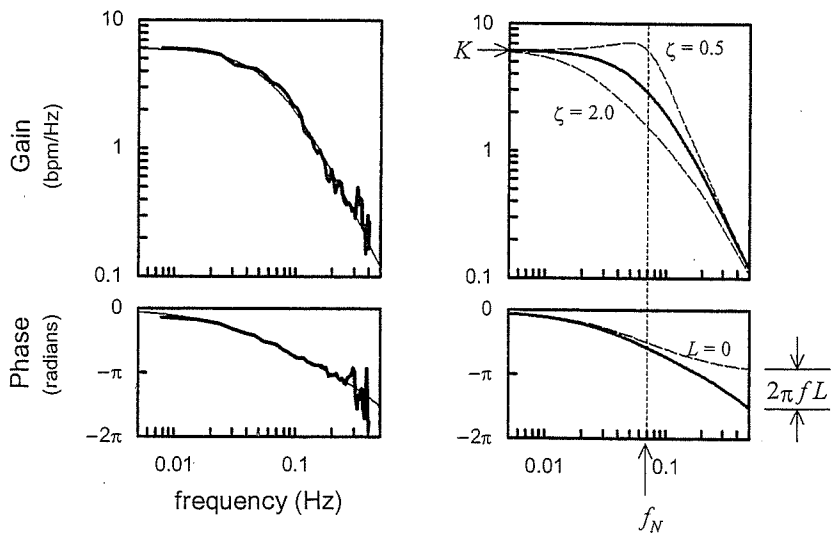

Fig. 8. A: Typical transfer function from SNS to HR obtained under control conditions (NA_0) in one animal. The thin smooth curve is a best-fit mathematical model for the transfer function. **B**: Schematic explanation of the model parameters. *K*: dynamic gain; f_N: natural frequency; ζ: damping ratio; *L*: pure dead time.

plasma catecholamine levels in conscious dogs. Am J Physiol Heart Circ Physiol. 1985;248:H82-8.
15. Novi AM. An electron microscope study of the innervation of papillary muscles in the rat. Anat Rec. 1968;160:123-41.
16. Yamaguchi N, de Champlain J, Nadeau R. Correlation between the response of the heart to sympathetic stimulation and the release of endogenous catecholamines into the coronary sinus of the dog. Circ Res. 1975;36:662-8.
17. Kawada T, Yamazaki T, Akiyama T, Shishido T, Miyano H, Sato T, Sugimachi M, Alexander J Jr, Sunagawa K. Interstitial norepinephrine level by cardiac microdialysis correlates with ventricular contractility. Am J Physiol Heart Circ Physiol. 1997;273:H1107-12.
18. Iversen LL. The uptake of catechol amines at high perfusion concentrations in the rat isolated heart: a novel catecholamine uptake process. Brit J Pharmacol. 1965;25:183-33.
19. Iversen LL. Uptake processes for biogenic amines. In: Iversen LL, Iversen SD, Snyder SH, editors. Handbook of Psychopharmacology, Section 1, Vol 3. New York: Plenum Press; 1975. p. 381-442.
20. Friedgen B, Halbrügge T, Graefe K. Role of uptake$_1$ and catechol-O-methyltransferase in removal of circulating catecholamines in the rabbit. Am J Physiol Endocrinol Metab. 1994;267:E814-21.
21. Boudreau G, Péronnet F, de Champlain J, Nadeau R. Presynaptic effects of epinephrine on norepinephrine release from cardiac sympathetic nerves in dogs. Am J Physiol Heart Circ Physiol. 1993;265:H205-11.
22. Esler M, Jennings G, Lambert G, Meredith I, Horne M, Eisenhofer G. Overflow of catecholamine neurotransmitters to the circulation: source, fate, and functions. Physiol Rev. 1990;70:963-85.
23. Schmidt H, Schurr C, Hedler L, Majewski H. Local modulation of norepinephrine release in vivo: Presynaptic β_2-adrenoceptors and endogenous adrenaline. J Cardiovasc Pharmacol. 1984;6:641-9.
24. Kawada T, Sugimachi M, Shidhido T, Miyano H, Sato T, Yoshimura R, Miyashita H, Nakahara T, Alexander J Jr, Sunagawa K. Simultaneous identification of static and dynamic vagosympathetic interactions in regulating heart rate. Am J Physiol Regul Integr Comp Physiol. 1999;276:R782-9.
25. Kawada T, Miyamoto T, Uemura K, Kashihara K, Kamiya K, Sugimachi M, Sunagawa K. Effects of neuronal norepinephrine uptake blockade on baroreflex neural and peripheral arc transfer characteristics. Am J Physiol Regul Integr Comp Physiol. 2004;286:R1110-20.

Am J Physiol Heart Circ Physiol 291: H2187–H2191, 2006.
First published June 9, 2006; doi:10.1152/ajpheart.00175.2006.

Effects of Ca^{2+} channel antagonists on nerve stimulation-induced and ischemia-induced myocardial interstitial acetylcholine release in cats

Toru Kawada,[1] Toji Yamazaki,[2] Tsuyoshi Akiyama,[2] Kazunori Uemura,[1] Atsunori Kamiya,[1] Toshiaki Shishido,[1] Hidezo Mori,[2] and Masaru Sugimachi[1]

[1]*Department of Cardiovascular Dynamics, Advanced Medical Engineering Center, National Cardiovascular Center Research Institute and* [2]*Department of Cardiac Physiology, National Cardiovascular Center Research Institute, Osaka, Japan*

Submitted 17 February 2006; accepted in final form 7 June 2006

Kawada, Toru, Toji Yamazaki, Tsuyoshi Akiyama, Kazunori Uemura, Atsunori Kamiya, Toshiaki Shishido, Hidezo Mori, and Masaru Sugimachi. Effects of Ca^{2+} channel antagonists on nerve stimulation-induced and ischemia-induced myocardial interstitial acetylcholine release in cats. *Am J Physiol Heart Circ Physiol* 291: H2187–H2191, 2006. First published June 9, 2006; doi:10.1152/ajpheart.00175.2006.—Although an axoplasmic Ca^{2+} increase is associated with an exocytotic acetylcholine (ACh) release from the parasympathetic postganglionic nerve endings, the role of voltage-dependent Ca^{2+} channels in ACh release in the mammalian cardiac parasympathetic nerve is not clearly understood. Using a cardiac microdialysis technique, we examined the effects of Ca^{2+} channel antagonists on vagal nerve stimulation- and ischemia-induced myocardial interstitial ACh releases in anesthetized cats. The vagal stimulation-induced ACh release [22.4 nM (SD 10.6), $n = 7$] was significantly attenuated by local administration of an N-type Ca^{2+} channel antagonist ω-conotoxin GVIA [11.7 nM (SD 5.8), $n = 7$, $P = 0.0054$], or a P/Q-type Ca^{2+} channel antagonist ω-conotoxin MVIIC [3.8 nM (SD 2.3), $n = 6$, $P = 0.0002$] but not by local administration of an L-type Ca^{2+} channel antagonist verapamil [23.5 nM (SD 6.0), $n = 5$, $P = 0.758$]. The ischemia-induced myocardial interstitial ACh release [15.0 nM (SD 8.3), $n = 8$] was not attenuated by local administration of the L-, N-, or P/Q-type Ca^{2+} channel antagonists, by inhibition of Na^+/Ca^{2+} exchange, or by blockade of inositol 1,4,5-trisphosphate [Ins(1,4,5)P_3] receptor but was significantly suppressed by local administration of gadolinium [2.8 nM (SD 2.6), $n = 6$, $P = 0.0283$]. In conclusion, stimulation-induced ACh release from the cardiac postganglionic nerves depends on the N- and P/Q-type Ca^{2+} channels (with a dominance of P/Q-type) but probably not on the L-type Ca^{2+} channels in cats. In contrast, ischemia-induced ACh release depends on nonselective cation channels or cation-selective stretch activated channels but not on L-, N-, or P/Q type Ca^{2+} channels, Na^+/Ca^{2+} exchange, or Ins(1,4,5)P_3 receptor-mediated pathway.

cardiac microdialysis; ω-conotoxin GVIA; ω-conotoxin MVIIC; KB-R7943; verapamil; vagal stimulation

ALTHOUGH N-TYPE Ca^{2+} CHANNELS play a dominant role in norepinephrine release from sympathetic nerve endings (8, 33, 34), the type(s) of Ca^{2+} channels controlling ACh release in the mammalian parasympathetic system is not fully understood and show diversity among reports. To name a few, in isolated parasympathetic submandibular ganglia from the rat, neurotransmission is mediated by Ca^{2+} channels that are resistant to the L-, N-, P/Q-, and R- type Ca^{2+} channel antagonists (29). When the negative inotropic response to field stimulation was examined in the isolated guinea pig atria, Hong and Chang (8) reported the importance of P/Q-type Ca^{2+} channels, whereas Serone et al. (28) reported the importance of N-type Ca^{2+} channels. Because field stimulation in the isolated preparations could induce responses different from those in the in vivo conditions, we aimed to examine the effects of Ca^{2+} channel antagonists on the vagal nerve stimulation-induced myocardial interstitial ACh release in the in vivo feline heart.

Aside from the important role of the normal physiological regulation of the heart, the vagal nerve can be a therapeutic target for certain cardiovascular diseases (2, 3, 13, 22, 27). In previous studies, we have shown that acute myocardial ischemia causes myocardial interstitial ACh release in the ischemic region independently of efferent vagal nerve activity (12, 14). The comparison of the effects of Ca^{2+} channel antagonists on the ACh releases induced by vagal nerve stimulation and by acute myocardial ischemia may deepen our understanding about the ischemia-induced myocardial interstitial ACh release.

A cardiac microdialysis technique offers detailed analyses of in vivo myocardial interstitial ACh release (1, 15). Because the local administration of pharmacological agents through a dialysis probe can modulate ACh release without significantly affecting systemic hemodynamics, a combination of cardiac microdialysis with local pharmacological interventions is useful for analyzing the mechanisms of ACh release in vivo. In the present study, we examined the effects of Ca^{2+} channel antagonists on nerve stimulation- and ischemia-induced ACh releases in anesthetized cats. The results indicate that stimulation-induced ACh release from the cardiac parasympathetic postganglionic nerves depends on the N- and P/Q-type Ca^{2+} channels but probably not on the L-type Ca^{2+} channels. In contrast, ischemia-induced myocardial interstitial ACh release is resistant to the inhibition of L-, N-, and P/Q-type Ca^{2+} channels. In addition, the ischemia-induced myocardial ACh release is resistant to the inhibition of Na^+/Ca^{2+} exchanger and the blockade of inositol 1,4,5-trisphosphate [Ins(1,4,5)P_3] receptor but is suppressed by gadolinium, suggesting that nonselective cation channels or cation-selective stretch-activated channels are involved.

MATERIALS AND METHODS

Common Preparation

Animal care was provided in accordance with the *Guiding Principles for the Care and Use of Animals in the Field of Physiological*

Address for reprint requests and other correspondence: T. Kawada, Dept. of Cardiovascular Dynamics, Advanced Medical Engineering Center, National Cardiovascular Center Research Institute, 5-7-1 Fujishirodai, Suita, Osaka 565-8565, Japan (e-mail: torukawa@res.ncvc.go.jp).

The costs of publication of this article were defrayed in part by the payment of page charges. The article must therefore be hereby marked "*advertisement*" in accordance with 18 U.S.C. Section 1734 solely to indicate this fact.

Sciences approved by the Physiological Society of Japan. All protocols were approved by the Animal Subjects Committee of the National Cardiovascular Center. Adult cats weighing from 2.2 to 4.2 kg were anesthetized via an intraperitoneal injection of pentobarbital sodium (30–35 mg/kg) and ventilated mechanically with room air mixed with oxygen. The depth of anesthesia was maintained with a continuous intravenous infusion of pentobarbital sodium (1–2 $mg \cdot kg^{-1} \cdot h^{-1}$) through a catheter inserted from the right femoral vein. Systemic arterial pressure was monitored from a catheter inserted from the right femoral artery. The vagi were sectioned bilaterally at the neck. The esophageal temperature of the animal, which was measured by a thermometer (CTM-303, TERUMO, Japan), was maintained at around 37°C using a heated pad and a lamp.

With the animal in the lateral position, the left fifth and sixth ribs were resected to expose the heart. A dialysis probe was implanted transversely, using a fine guiding needle, into the anterolateral free wall of the left ventricle perfused by the left anterior descending coronary artery (LAD). Heparin sodium (100 U/kg) was administered intravenously to prevent blood coagulation. At the end of the experiment, the experimental animals were killed with an overdose of pentobarbital sodium. Postmortem examination confirmed that the dialysis probe had been threaded in the middle layer of the left ventricular myocardium. The thickness of the left ventricular free wall was ~7–8 mm, and the semipermeable membrane of the dialysis probe was positioned ~3–4 mm from the epicardial surface.

Dialysis Technique

The materials and properties of the dialysis probe have been described previously (1). Briefly, we designed a transverse dialysis probe. A dialysis fiber of semipermeable membrane (13 mm length, 310 μm OD, 200 μm ID; PAN-1200, 50,000 molecular weight cutoff, Asahi Chemical, Japan) was glued at both ends to polyethylene tubes (25 cm length, 500 μm OD, 200 μm ID). The dialysis probe was perfused at a rate of 2 μl/min with Ringer solution containing a cholinesterase inhibitor eserine (physostigmine, 100 μM). Experimental protocols were started 2 h after the dialysis probe was implanted when the ACh concentration in the dialysate reached a steady state. The ACh concentration in the dialysate was measured by high-performance liquid chromatography with electrochemical detection (Eicom, Kyoto, Japan).

Local administration of a pharmacological agent was carried out through a dialysis probe. That is to say, we added the pharmacological agent to the perfusate and allowed 1 h for a settling time. The pharmacological agent should spread around the semipermeable membrane, thereby affecting the neurotransmitter release in the vicinity of the semipermeable membrane. Because the distribution across the semipermeable membrane is required, based on previous results (33, 34), we used the pharmacological agent at the concentration 10–100 times higher than that required for complete channel blockade in experimental settings in vitro.

Specific Preparation and Protocols

Protocol 1. Bipolar platinum electrodes were attached bilaterally to the cardiac ends of the sectioned vagi at the neck. The nerves and electrodes were covered with warmed mineral oil for insulation. The vagal nerves were stimulated for 15 min (20 Hz, 1 ms, 10 V). We measured the stimulation-induced ACh release in the absence of Ca^{2+} channel blockade (control, $n = 7$) and examined the effects of an L-type Ca^{2+} channel antagonist verapamil (100 μM, $n = 5$), an N-type Ca^{2+} channel antagonist ω-conotoxin GVIA (10 μM, $n = 7$), a P/Q-type Ca^{2+} channel antagonist ω-conotoxin MVIIC (10 μM, $n = 6$), and combined administration of ω-conotoxin GVIA and ω-conotoxin MVIIC (10 μM each, $n = 6$).

Protocol 2. Because a preliminary result from *protocol 1* suggested that local administration of verapamil was ineffective in suppressing stimulation-induced ACh release, we examined the effects of the intravenous administration of verapamil (300 μg/kg, $n = 6$) on stimulation-induced ACh release in vagotomized animals as a supplemental experiment.

Protocol 3. A 60-min LAD occlusion was performed by using a 3-0 silk suture passed around the LAD just distal to the first diagonal branch. We measured the ACh levels during 45–60 min of ischemia in the absence of Ca^{2+} channel blockade (control, $n = 8$) and examined the effects of verapamil (100 μM, $n = 5$), ω-conotoxin GVIA (10 μM, $n = 5$), and ω-conotoxin MVIIC (10 μM, $n = 5$). A previous result indicated that the ischemia-induced ACh release reached the steady state during 45–60 min of ischemia (14). We also examined the effects of three additional agents, a Na^+/Ca^{2+} exchange inhibitor KB-R7943 (10 μM, $n = 5$) (9, 10), an $Ins(1,4,5)P_3$ receptor blocker xestospongin C (500 μM, $n = 6$) (25), and a nonselective cation channel blocker or a cation-selective stretch activated channel blocker gadolinium (1 mM) (5, 17), on the ischemia-induced ACh release.

Statistical Analysis

All data are presented as mean (SD) values. In *protocol 1*, we compared stimulation-induced ACh release among the five groups using one-way analysis of variance followed by the Student-Neuman-Keuls test (6). In *protocol 2*, we used an unpaired-*t* test (two-sided) to examine the effect of intravenous verapamil administration on stimulation-induced ACh release. In *protocol 3*, we compared ischemia-induced ACh release among the seven groups using one-way analysis of variance followed by the Dunnett' test against the control. For all analyses, differences were considered significant when $P < 0.05$.

RESULTS

In *protocol 1*, the ACh level during electrical vagal stimulation was 22.4 nM (SD 10.6). Local administration of verapamil did not affect stimulation-induced ACh release (Fig. 1). In contrast, local administration of ω-conotoxin GVIA or ω-conotoxin MVIIC suppressed stimulation-induced ACh release. The extent of suppression was greater in the latter. The ACh level was significantly lower in the simultaneous administration group (ω-conotoxin GVIA + ω-conotoxin MVIIC)

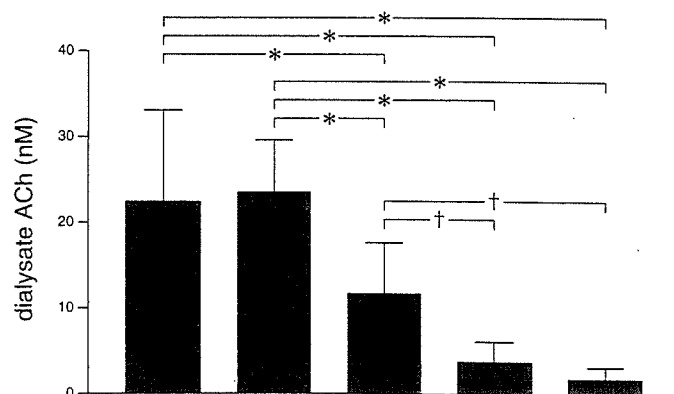

	vehicle	verapamil	ω-CTX GVIA	ω-CTX MVIIC	ω-CTX MVIIC + ω-CTX GVIA
vehicle		0.758	*0.0054*	*0.0002*	*0.0002*
verapamil	0.758		*0.0068*	*0.0002*	*0.0001*
GVIA	*0.0054*	*0.0068*		*0.033*	*0.025*
MVIIC	*0.0002*	*0.0002*	*0.033*		0.581
MVIIC+GVIA	*0.0002*	*0.0001*	*0.025*	0.581	

Fig. 1. Effects of local administration of verapamil, ω-conotoxin GVIA, ω-conotoxin MVIIC, or ω-conotoxin GVIA plus ω-conotoxin MVIIC on vagal nerve stimulation-induced myocardial interstitial ACh release. Both ω-conotoxin GVIA and ω-conotoxin MVIIC, but not verapamil, suppressed stimulation-induced ACh release. Data are mean (SD) values. *$P < 0.01$, †$P < 0.05$. The exact P values are presented.

than that in the ω-conotoxin GVIA group but was not different from the ω-conotoxin MVIIC group.

In *protocol 2*, the intravenous administration of verapamil did not significantly change stimulation-induced ACh release [21.7 nM (SD 12.8)] compared with the control group (P = 0.91).

In *protocol 3*, the ACh level in the ischemic region was 14.9 nM (SD 8.3) during 45–60 min of acute myocardial ischemia. Inhibition of voltage-dependent Ca^{2+} channels by local administration of verapamil, ω-conotoxin GVIA, or ω-conotoxin MVIIC did not affect ischemia-induced ACh release (Fig. 2). Inhibition of the reverse mode action of Na^+/Ca^{2+} exchange by local administration of KB-R7943 appeared to have augmented rather than suppressed ischemia-induced ACh release, though there was no statistically significant difference from the control. Blockade of the Ins(1,4,5)P_3 receptor by local administration of xestospongin C did not affect the ischemia-induced ACh release. In contrast, blockade of nonselective cation channels or cation-selective stretch-activated channels by local administration of gadolinium suppressed the ischemia-induced ACh release.

DISCUSSION

Ca^{2+} Channels Involved in Stimulation-Induced ACh Release

Although neurotransmitter release at mammalian sympathetic neuroeffector junctions predominantly depends on Ca^{2+} influx through N-type Ca^{2+} channels (23, 33, 34), the type(s) of Ca^{2+} channels involved in ACh release from cardiac parasympathetic neuroeffector junctions show diversity among reports (8, 28). One possible factor hampering investigations into parasympathetic postganglionic neurotransmitter release in response to vagal nerve stimulation in vivo is that the parasympathetic ganglia are usually situated in the vicinity of the effector organs, thereby making it difficult to separately assess ACh release from preganglionic and postganglionic nerves. In the previous study from our laboratory, intravenous administration, but not local administration of a ganglionic blocker, hexamethonium reduced vagal stimulation-induced ACh release assessed by cardiac microdialysis (1). The negligible effect of local hexamethonium administration on stimulation-induced ACh release suggests the lack of parasympathetic ganglia around the dialysis probe. In support of our speculation, a recent neuroanatomical finding indicates that three ganglia, away from the left anterior free wall targeted by the dialysis probe, provide the major source for left ventricular postganglionic innervation in cats: a cranioventricular ganglion, a left ventricular ganglion 2 (so designated), and an interventriculo-septal ganglion (11). Therefore, ACh, as measured by cardiac microdialysis, is considered to predominantly reflect ACh release from parasympathetic postganglionic nerves.

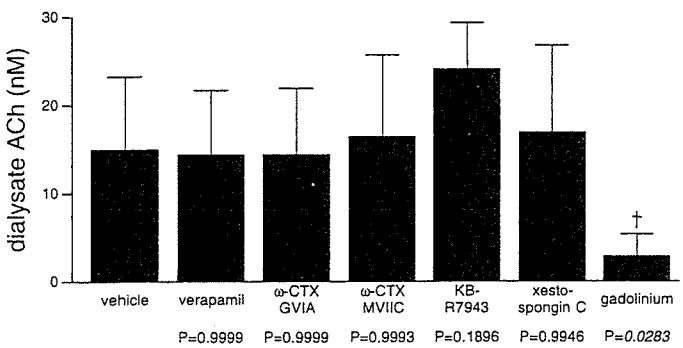

Fig. 2. Effects of local administration of verapamil, ω-conotoxin GVIA, ω-conotoxin MVIIC, KB-R7943, xestospongin C, or gadolinium on acute myocardial ischemia-induced myocardial interstitial ACh release in the ischemic region. Gadolinium alone suppressed the ischemia-induced ACh release. Data are mean (SD) values. †$P < 0.05$. The exact P values are presented.

Local (*protocol 1*) or intravenous (*protocol 2*) administration of verapamil did not affect stimulation-induced ACh release. In contrast, vagal stimulation-induced ACh release was reduced in both the ω-conotoxin GVIA and ω-conotoxin MVIIC groups but to a greater extent in the latter (Fig. 1). Therefore, both N- and P/Q-type, but probably not L-type, Ca^{2+} channels are involved in stimulation-induced ACh release from the cardiac parasympathetic postganglionic nerves in cats. The contribution of P/Q type Ca^{2+} channels to ACh release might be greater than that of N-type Ca^{2+} channels. Hong and Chang (8) reported that the negative inotropic response to field stimulation depends predominantly on the P/Q-type Ca^{2+} channels in isolated guinea pig atria, whereas Serone et al. (28) reported the predominance of N-type Ca^{2+} channels. In those studies, the field stimulation employed differed from ordinary activation of the postganglonic nerves by nerve discharge and, in addition, ACh release was not directly measured. The present study directly demonstrated the involvement of P/Q- and N-type Ca^{2+} channels in the stimulation-induced ACh release in the cardiac parasympathetic postganglionic nerves. These results support the concept that multiple subtypes of the voltage-gated Ca^{2+} channel mediate transmitter release from the same population of parasympathetic neurons (31).

Stimulation-induced ACh release was suppressed by ~50% in the ω-conotoxin GVIA group and by ~80% in the ω-conotoxin MVIIC group. The algebraic summation of the extent of suppression exceeded 100%. The phenomenon may be in part due to the nonlinear dose-response relationship between Ca^{2+} influx and transmitter release (32). The supra-additive phenomenon may be also due to the affinity of ω-conotoxin MVIIC to N-type Ca^{2+} channels (8, 26, 36). Combined local administration of ω-conotoxin GVIA and ω-conotoxin MVIIC almost completely suppressed stimulation-induced ACh release to a level similar to that achieved by the Na^+ channel inhibitor tetrodotoxin (15). Therefore, involvement of another untested type of Ca^{2+} channel(s) is unlikely in the stimulation-induced ACh release from the cardiac parasympathetic postganglionic nerves in cats.

Ca^{2+} Channels and Ischemia-Induced ACh Release

In a previous study, we showed that acute myocardial ischemia evokes myocardial interstitial ACh release in the ischemic region via a local mechanism independent of efferent vagal nerve activity (14). In that study, the inhibition of intracellular Ca^{2+} mobilization by local administration of 3,4,5-trimethoxybenzoic acid 8-(diethyl amino)-octyl ester (TMB-8) suppressed ischemia-induced ACh release, suggesting that an axoplasmic Ca^{2+} elevation is essential for the ischemia-induced ACh release. Because tissue K^+ concentration increases in the ischemic region (7, 18), high K^+-induced

depolarization could activate voltage-dependent Ca^{2+} channels even in the absence of efferent vagal nerve activity. However, ischemia-induced ACh release was not suppressed by local administration of verapamil, ω-conotoxin GVIA, or ω-conotoxin MVIIC (Fig. 2). Therefore, Ca^{2+} entry through the voltage-dependent Ca^{2+} channels is unlikely a mechanism for the ischemia-induced myocardial interstitial ACh release.

Acute myocardial ischemia causes energy depletion in the ischemic region, which impairs Na^+-K^+-ATPase activity. Ischemia also causes acidosis in the ischemic region, which promotes Na^+/H^+ exchange. As a result, ischemia causes intracellular Na^+ accumulation. The decrease in the Na^+ gradient across the plasma membrane may then cause the Na^+/Ca^{2+} exchanger to operate in the reverse mode, facilitating intracellular Ca^{2+} overload. KB-R7943 can inhibit the reverse mode of Na^+/Ca^{2+} exchange (9, 10) and its potential to protect against ischemia-reperfusion injury has been reported (21). In the present study, however, local administration of KB-R7943 failed to suppress and rather increased ACh release during ischemia as opposed to our expectation. It is plausible that the inhibition of reverse mode of Na^+/Ca^{2+} may have facilitated the accumulation of intracellular Na^+ and induced adverse effects that cancelled the possible beneficial effects derived from the inhibition of Ca^{2+} entry through the Na^+/Ca^{2+} exchanger itself. In addition, KB-R7943 could inhibit the forward mode of Na^+/Ca^{2+} exchange and reduce Ca^{2+} efflux (16), contributing to the intracellular Ca^{2+} accumulation and ACh release. In the present study, we observed the effects of KB-R7943 only during the ischemic period. However, accumulation of intracellular Na^+ through Na^+/H^+ exchange is enhanced on reperfusion due to the washout of extracellular H^+ (20). The inhibition of Na^+/Ca^{2+} exchange to suppress Ca^{2+} overload might become more important during the reperfusion phase. For instance, the percent segment shortening of the left ventricle was improved by KB-R7943 during reperfusion but not during ischemia (35).

As already mentioned, the ischemia-induced ACh release can be blocked by TMB-8 and thus the intracellular Ca^{2+} mobilization is required for the ischemia-induced ACh release (14). Besides the Ca^{2+} entries through voltage-dependent Ca^{2+} channels and via the reverse mode of Na^+/Ca^{2+} exchanger, Ca^{2+} may be mobilized from the endoplasmic reticulum via pathological pathways. As an example, the mitochondrial permeability transition pore triggered in pathological conditions is linked to cytochrome *c* release. Cytochrome *c* can bind to the endoplasmic reticulum Ins(1,4,5)P_3 receptor, rendering the channel insensitive to autoinhibition by high cytosolic Ca^{2+} concentration and resulting in enhanced endoplasmic reticulum Ca^{2+} release (4, 30). In the present study, however, blockade of Ins(1,4,5)P_3 receptor by xestospongin C failed to suppress the ischemia-induced ACh release. In contrast, local administration of gadolinium significantly suppressed the ischemia-induced ACh release. Therefore, nonselective cation channels or cation-selective stretch-activated channels contribute to the ischemia-induced ACh release. During myocardial ischemia, the ischemic region can be subjected to paradoxical systolic bulging. Such bulging likely opens stretch-activated channels and causes myocardial interstitial ACh release, possibly leading to cardioprotection by ACh against ischemic injury (2).

Limitations

First, the experiment was performed under anesthetic conditions, which may have influenced basal autonomic activity. However, because we sectioned the vagi at the neck, basal autonomic activity may have had only a minor effect on ACh release during the vagal stimulation and during acute myocardial ischemia. Second, we added eserine to the perfusate to inhibit immediate degradation of ACh (24), which may have increased the ACh level in the synaptic cleft and activated regulatory pathways such as autoinhibition of ACh release via muscarinic receptors (24). However, the myocardial interstitial ACh level measured under this condition could reflect changes induced by Na^+ channel inhibitor, choline uptake inhibitor, and vesicular ACh transport inhibitor as described in a previous study (15). Therefore, we think that the interpretation of the present results is reasonable. Third, tissue and species differences should be taken into account when extrapolating the present findings, because significant heterogeneity in the Ca^{2+} channels involved in the mammalian parasympathetic system may exist. Finally, we used verapamil to test the involvement of L-type Ca^{2+} channels in the ACh release. There are three major types of L-type Ca^{2+} channel antagonists with different binding domains (verapamil, nifedipine, and diltiazem) (19). Whether the effects on the ACh release are common among the three types of L-type Ca^{2+} channel antagonists remains unanswered.

In conclusion, the N- and P/Q-type Ca^{2+} channels (with the P/Q-type dominant), but probably not the L-type Ca^{2+} channels, are involved in vagal stimulation-induced ACh release from the cardiac parasympathetic postganglionic nerves in cats. In contrast, myocardial interstitial ACh release in the ischemic myocardium is resistant to the blockade of L-, N-, and P/Q-type Ca^{2+} channels. In addition, the ischemia-induced myocardial ACh release is resistant to the inhibition of Na^+/Ca^{2+} exchanger and the blockade of Ins(1,4,5)P_3 receptor but is suppressed by gadolinium, suggesting that nonselective cation channels or cation-selective stretch-activated channels are involved.

GRANTS

This study was supported by Health and Labour Sciences Research Grant for Research on Advanced Medical Technology from the Ministry of Health, Labour and Welfare of Japan, Health and Labour Sciences Research Grant for Research on Medical Devices for Analyzing, Supporting and Substituting the Function of Human Body from the Ministry of Health, Labour and Welfare of Japan, Health and Labour Sciences Research Grant H18-Iryo-Ippan-023 from the Ministry of Health, Labour and Welfare of Japan, Program for Promotion of Fundamental Studies in Health Science from the National Institute of Biomedical Innovation, a Grant provided by the Ichiro Kanehara Foundation, Ground-based Research Announcement for Space Utilization promoted by Japan Space Forum, and Industrial Technology Research Grant Program in 03A47075 from New Energy and Industrial Technology Development Organization of Japan.

REFERENCES

1. **Akiyama T, Yamazaki T, and Ninomiya I.** In vivo detection of endogenous acetylcholine release in cat ventricles. *Am J Physiol Heart Circ Physiol* 266: H854–H860, 1994.
2. **Ando M, Katare RG, Kakinuma Y, Zhang D, Yamasaki F, Muramoto K, and Sato T.** Efferent vagal nerve stimulation protects heart against ischemia-induced arrhythmias by preserving connexin43 protein. *Circulation* 112: 164–170, 2005.

3. **Bibevski S and Dunlap ME.** Prevention of diminished parasympathetic control of the heart in experimental heart failure. *Am J Physiol Heart Circ Physiol* 287: H1780–H1785, 2004.
4. **Brookes PS, Yoon Y, Robotham JL, Anders MW, and Sheu SS.** Calcium, ATP, and ROS: a mitochondrial love-hate triangle. *Am J Physiol Cell Physiol* 287: C817–C833, 2004.
5. **Caldwell RA, Clemo HF, and Baumgarten CM.** Using gadolinium to identify stretch-activated channels: technical considerations. *Am J Physiol Cell Physiol* 275: C619–C621, 1998.
6. **Glantz SA.** *Primer of Biostatistics* (5th ed) New York: McGraw-Hill, 2002.
7. **Hirche HJ, Franz CHR, Bös L, Bissig R, Lang R, and Schramm M.** Myocardial extracellular K^+ and H^+ increase and noradrenaline release as possible cause of early arrhythmias following acute coronary artery occlusion in pigs. *J Mol Cell Cardiol* 12: 579–593, 1979.
8. **Hong SJ and Chang CC.** Calcium channel subtypes for the sympathetic and parasympathetic nerves of guinea-pig atria. *Br J Pharmacol* 116: 1577–1582, 1995.
9. **Iwamoto T, Kita S, Uehara A, Inoue Y, Taniguchi Y, Imanaga I, and Shigekawa M.** Structural domains influencing sensitivity to isothiourea derivative inhibitor KB-R7943 in cardiac Na^+/Ca^{2+} exchanger. *Mol Pharmacol* 59: 524–531, 2001.
10. **Iwamoto T, Watano T, and Shigekawa M.** A novel isothiourea derivative selectively inhibits the reverse mode of Na^+/Ca^{2+} exchange in cells expressing NCX1. *J Biol Chem* 271: 22391–22397, 1996.
11. **Johnson TA, Gray AL, Lauenstein JM, Newton SS, and Massari VJ.** Parasympathetic control of the heart. I. An interventriculo-septal ganglion is the major source of the vagal intracardiac innervation of the ventricles. *J Appl Physiol* 96: 2265–2272, 2004.
12. **Kawada T, Yamazaki T, Akiyama T, Inagaki M, Shishido T, Zheng C, Yanagiya Y, Sugimachi M, and Sunagawa K.** Vagosympathetic interactions in ischemia-induced myocardial norepinephrine and acetylcholine release. *Am J Physiol Heart Circ Physiol* 280: H216–H221, 2001.
13. **Kawada T, Yamazaki T, Akiyama T, Li M, Ariumi H, Mori H, Sunagawa K, and Sugimachi M.** Vagal stimulation suppresses ischemia-induced myocardial interstitial norepinephrine release. *Life Sci* 78: 882–887, 2006.
14. **Kawada T, Yamazaki T, Akiyama T, Sato T, Shishido T, Inagaki M, Takaki H, Sugimachi M, and Sunagawa K.** Differential acetylcholine release mechanisms in the ischemic and non-ischemic myocardium. *J Mol Cell Cardiol* 32: 405–414, 2000.
15. **Kawada T, Yamazaki T, Akiyama T, Shishido T, Inagaki M, Uemura K, Miyamoto T, Sugimachi M, Takaki H, and Sunagawa K.** In vivo assessment of acetylcholine-releasing function at cardiac vagal nerve terminals. *Am J Physiol Heart Circ Physiol* 281: H139–H145, 2001.
16. **Kimura J, Watano T, Kawahara M, Sakai E, and Yatabe J.** Direction-independent block of bi-directional Na^+/Ca^{2+} exchange current by KB-R7943 in guinea-ping cardiac myocytes. *Br J Pharmacol* 128: 969–974, 1999.
17. **Kimura S, Mieno H, Tamaki K, Inoue M, and Chayama K.** Nonselective cation channel as a Ca^{2+} influx pathway in pepsinogen-secreting cells of bullfrog esophagus. *Am J Physiol Gastrointest Liver Physiol* 281: G333–G341, 2001.
18. **Kléber AG.** Extracellular potassium accumulation in acute myocardial ischemia. *J Mol Cell Cardiol* 16: 389–394, 1984.
19. **Kurokawa J, Adachi-Akahane S, and Nagao T.** 1–5-Benzothiazepine binding domain is located on the extracellular side of the cardiac L-type Ca^{2+} channel. *Mol Pharmacol* 51: 262–268, 1997.
20. **Lazdunski M, Frelin C, and Vigne P.** The sodium/hydrogen exchange system in cardiac cells: its biochemical and pharmacological properties and its role in regulating internal concentrations of sodium and internal pH. *J Mol Cell Cardiol* 17: 1029–1042, 1985.
21. **Lee C, Dhalla NS, and Hryshko LV.** Therapeutic potential of novel Na^+-Ca^{2+} exchange inhibitors in attenuating ischemia-reperfusion injury. *Can J Cardiol* 21: 509–516, 2005.
22. **Li M, Zheng C, Sato T, Kawada T, Sugimachi M, and Sunagawa K.** Vagal nerve stimulation markedly improves long-term survival after chronic heart failure in rats. *Circulation* 109: 120–124, 2004.
23. **Molderings GJ, Likungu J, and Göthert M.** N-type calcium channels control sympathetic neurotransmission in human heart atrium. *Circulation* 101: 403–407, 2000.
24. **Nicholls DG.** *Proteins, Transmitters and Synapses.* Oxford: Blackwell Science, 1994.
25. **Oka T, Sato K, Hori M, Ozaki H, and Karaki H.** Xestospongin C, a novel blocker of IP_3 receptor, attenuates the increase in cytosolic calcium level and degranulation that is induced by antigen in RBL-2H3 mast cells. *Br J Pharmacol* 135: 1959–1966, 2002.
26. **Randall A and Tsien RW.** Pharmacological dissection of multiple types of Ca^{2+} channel currents in rat cerebellar granule neurons. *J Neurosci* 15: 2995–3012, 1995.
27. **Schauerte P, Scherlag BJ, Scherlag MA, Goli S, Jackman WM, and Lazzara R.** Ventricular rate control during atrial fibrillation by cardiac parasympathetic nerve stimulation: a transvenous approach. *J Am Coll Cardiol* 34: 2043–2050, 1999.
28. **Serone AP and Angus JA.** Role of N-type calcium channels in autonomic neurotransmission in guinea-pig isolated left atria. *Br J Pharmacol* 127: 927–934, 1999.
29. **Smith AB, Motin L, Lavidis NA, and Adams DJ.** Calcium channels controlling acetylcholine release from preganglionic nerve terminals in rat autonomic ganglia. *Neuroscience* 95: 1121–1127, 2000.
30. **Verkhratsky A and Toescu EC.** Endoplasmic reticulum Ca^{2+} homeostasis and neuronal death. *J Cell Mol Med* 4: 351–361, 2003.
31. **Waterman SA.** Multiple subtypes of voltage-gated calcium channel mediate transmitter release from parasympathetic neurons in the mouse bladder. *J Neurosci* 16: 4155–4161, 1996.
32. **Wheeler DB, Randall A, and Tsien RW.** Changes in action potential duration after reliance of excitatory synaptic transmission on multiple types of Ca^{2+} channels in rat hippocampus. *J Neurosci* 16: 2226–2237, 1996.
33. **Yahagi N, Akiyama T, and Yamazaki T.** Effects of ω-conotoxin GVIA on cardiac sympathetic nerve function: *J Auton Nerv Syst* 68: 43–48, 1998.
34. **Yamazaki T, Akiyama T, Kitagawa H, Takauchi Y, Kawada T, and Sunagawa K.** A new, concise dialysis approach to assessment of cardiac sympathetic nerve terminal abnormalities. *Am J Physiol Heart Circ Physiol* 272: H1182–H1187, 1997.
35. **Yoshitomi O, Akiyama D, Hara T, Cho S, Tomiyasu S, and Sumikawa K.** Cardioprotective effects of KB-R7943, a novel inhibitor of Na^+/Ca^{2+} exchanger, on stunned myocardium in anesthetized dogs. *J Anesth* 19: 124–130, 2005.
36. **Zhang JF, Randall AD, Ellinor PT, Horne WA, Sather WA, Tanabe T, Schwarz TL, and Tsien RW.** Distinctive pharmacology and kinetics of cloned neuronal Ca^{2+} channels and their possible counterparts in mammalian CNS neurons. *Neuropharmacology* 32: 1075–1088, 1993.

ELSEVIER

Journal of Neuroscience Methods 156 (2006) 71–75

JOURNAL OF NEUROSCIENCE METHODS

www.elsevier.com/locate/jneumeth

Reversible vagal blockade in conscious rats using a targeted delivery device

Can Zheng [a,*], Toru Kawada [a], Meihua Li [a], Takayuki Sato [b], Kenji Sunagawa [c], Masaru Sugimachi [a]

[a] *Department of Cardiovascular Dynamics, Advanced Medical Engineering Center, National Cardiovascular Center Research Institute, 5-7-1 Fujishirodai, Suita-shi, Osaka 565-8565, Japan*

[b] *Department of Physiology, Kochi Medical School, Kochi 783-8505, Japan*

[c] *Department of Cardiovascular Medicine, Graduate School of Medical Sciences, Kyushu University, Fukuoka 812-8582, Japan*

Received 30 November 2005; received in revised form 7 February 2006; accepted 8 February 2006

Abstract

Reversible methods of nerve blockade greatly aid neurophysiological and behavioral studies. We have developed an implantable device for the local delivery of anesthetics to the area surrounding the vagal nerve in rats. The device consists of a thick silicone tube for insulating the nerves from the surrounding tissue, and a thin silicone tube for the infusion of anesthetics into the insulating tube. The in vivo performance of the device was tested electrophysiologically, and cardiovascular responses to vagal stimulation were measured in conscious animals. Nerve conductivity was completely blocked by injection of a small amount (<20 μl) of 1% lidocaine, with conductivity subsequently recovering gradually after 10–40 min. Electrical stimulation of the right vagus nerve in conscious rats increased arterial pressure while decreasing heart rate. The local blockade of afferent fibers abolished the arterial pressure response but preserved the bradycardic response to vagal nerve stimulation. The targeted delivery device was useful for reversible vagal blockade in conscious rats.

Keywords: Vagus; Conduction blockade; Electric stimulation; Heart rate; Blood pressure; Conscious; Rat

1. Introduction

Peripheral nerves are the first step in the pathway that conducts signals from various peripheral sensors to the central nervous system (CNS) and are also the output pathway for signals from the CNS to various organs, with most peripheral nerves containing both afferent and efferent fibers. In the investigation of the integrative functions of the autonomic nervous system, several techniques have been developed for performing nerve blockade for recording or selectively stimulating either afferent or efferent fibers. One such technique is surgical denervation, which effectively eliminates nerve conduction, but is irreversible and may not be applicable to the vagus nerve in the chronic experimental settings, as animals cannot survive for long after bilateral vagotomy. Nerve cooling provides a reversible nerve blockade in conscious large animals (Derksen et al., 1981; Borgdorff and Versteeg, 1984; Cudd, 1998) and in anesthetized small animals (Vizek et al., 1983; Schultz et al., 1988; Lee et al., 1990), but is difficult in conscious small animals such as rats, due to technical problems associated with the size of the nerve cooling device. Alternatively, local anesthetics such as lidocaine are widely used for nerve blockade in clinical practice and animal studies (Thalhammer et al., 1995; Gokin et al., 2001; Potocnik et al., 2001). The major advantages of anesthetics for nerve blockade are the complete reversibility of the nerve blockade and the ease of administration. However, it can be difficult to administer local anesthetics in small conscious animals, largely because the vagus nerve runs close to the common carotid artery and the aortic depressor nerve, and therefore the injection procedure may result in artery or nerve damage. A technique of delivering neurotrophins or anesthetics to the sciatic nerve has been demonstrated in the conscious rat model (Kanje et al., 1988; Costanzo et al., 1999). However, it is not yet known whether such a targeted delivery method can be used to block the vagus nerve in conscious rats. In this study, we designed a targeted delivery device for the rat vagus nerve, which allowed local

* Corresponding author. Tel.: +81 6 6833 5012x2427; fax: +81 6 6835 5403.
E-mail address: zhengcan@ri.ncvc.go.jp (C. Zheng).

0165-0270/$ – see front matter © 2006 Elsevier B.V. All rights reserved.
doi:10.1016/j.jneumeth.2006.02.015

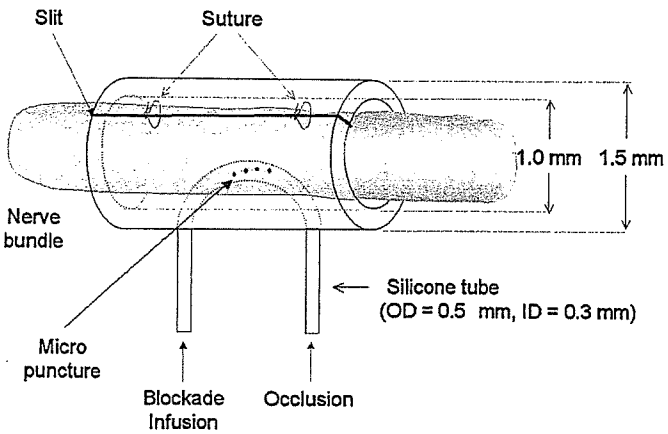

Fig. 1. Schematic illustration of the design of the targeted delivery device for the rat vagus nerve.

infusion of anesthetics into the area surrounding the nerve. The aim of this study was to evaluate this targeted delivery device for vagal blockade in conscious rats.

2. Materials and methods

2.1. A targeted delivery device

We designed an implantable device for delivering anesthetics to the area surrounding the rat cervical vagus nerve. As shown in Figs. 1 and 2E, this device was composed of a thick silicone tube (i.d. = 1.0 mm; o.d. = 1.5 mm; L = 3–4 mm) acting as a nerve guiding tube, and a thin silicone tube (i.d. = 0.3 mm; o.d. = 0.5 mm) for the injection of anesthetic agents. We made a longitudinal slit in the thick tube and pierced two holes in the wall of this tube for the thin tube to pass in and out of. Several micro-punctures were made by a microneedle (with a tip of 0.01 mm) in the inner part of the thin tube to allow the anesthetics to leak out into the guide tube.

We injected anesthetics slowly from one end of the thin tube until the liquid anesthetics replaced the air in the tube, and then we occluded the other end while increasing the pressure in the thin tube to force the liquid to leak out through the micro-punctures into the area surrounding the nerve. In the present study, we used 1% lidocaine solution for local blockade of vagal conduction. After completion of the experimental protocol, we flushed the tubes with distilled water to prevent the micro-punctures from becoming occluded by residual anesthetics.

2.2. Surgical preparation

Experiments were performed on six Sprague–Dawley rats weighing between 320 and 450 g. Animals were cared for in strict accordance with the Guiding Principles for the Care and Use of Animals in the Field of Physiological Science approved by the Physiological Society of Japan. Under 1.5%-halothane anesthesia, the lead wires of the cuff electrodes and the infusion tubes were tunneled subcutaneously from the back where they were fixed to a custom-designed multi-channel skin connector (Fig. 2B and G). The right vagus nerve was carefully dissected away from the common carotid artery and placed into the guide tube. The slit in the guide tube was then sutured by a polypropylene suture (8-0, ETHICON, INC.). Two custom-designed cuff electrodes, each having a pair of stainless steel wire electrodes (Fig. 2F), were implanted into the nerve trunk in the proximal and distal sides of the guide tube at a distance of 1.1–1.4 mm. Next, a blood pressure telemeter (TA11PA-C40, DSI) was implanted into the abdomen with a pressure sensor inserted into the abdominal aorta for monitoring mean arterial pressure (MAP) and heart rate (HR). After recovery from the surgical procedure, the animals were maintained on standard rat chow ad libitum, and were restrained in a rodent cage for physiological measurements as described below.

2.3. Experimental protocols

The experimental protocols were conducted at least 1 week after the implantation surgery. The in vivo effectiveness of the targeted delivery for nerve blockade was evaluated electrophysiologically and by measurement of HR and MAP responses to

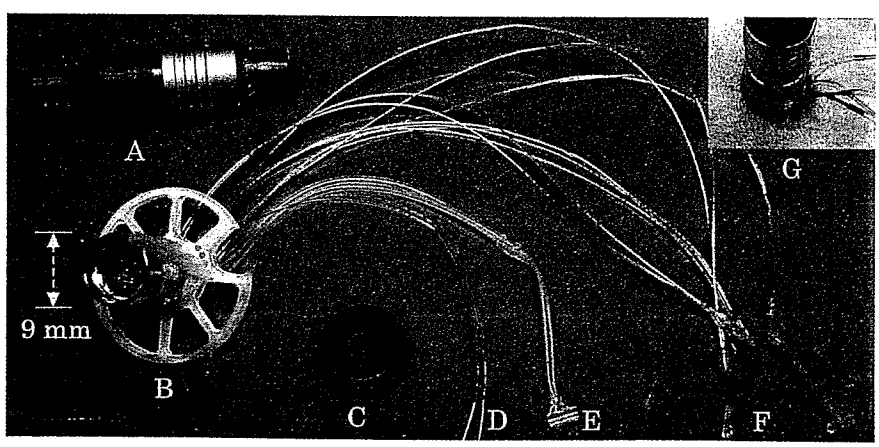

Fig. 2. Photographic images of the multi-channel skin connector with electrodes and nerve blocker. (A) Plug, (B) skin connector with 12-pin receptacle, (C) cap, (D) ECG leads, (E) nerve blocker, (F) nerve electrodes, the leads were extended with flexible coil (made of stainless wire of 0.03 mm in diameter, epoxy coated) and tips were fixed in the slit silicone tube (i.d. = 0.5; o.d. = 1 mm), and (G) implanted skin connector with local infusion setting.

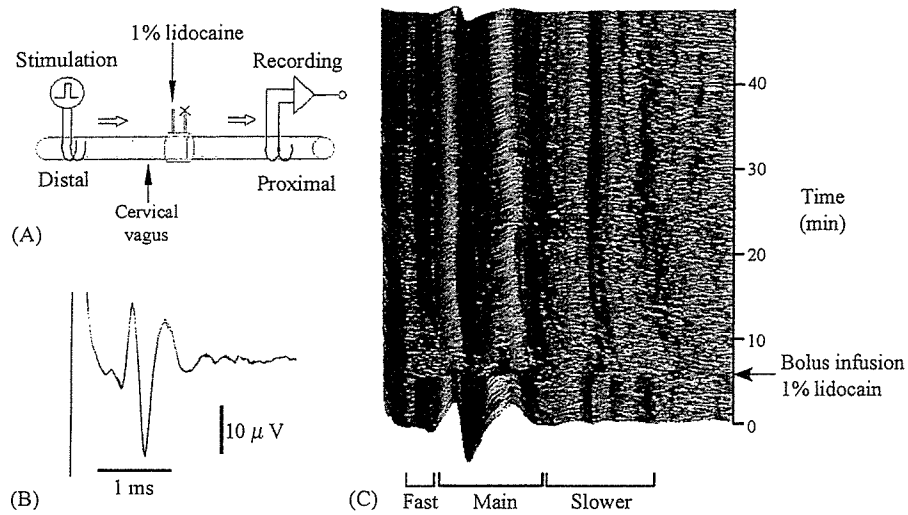

Fig. 3. Example of in vivo electrophysiology of the rat vagus. (A) A diagram of the experimental arrangement. (B) Compound action potential (CAP) of the right vagus evoked by the electrical pulse (1 Hz, 0.3 ms, 1.3 V). (C) The inhibition of vagal conduction by local injection of a small amount (<20 μl) of 1% lidocaine in conscious rats. Each trace was obtained as a result of waveform averaging of 10 single successive sweeps.

electrical stimulation of the vagus nerve in conscious animals. While the rat was loosely restrained in a rodent cage, lead wires for nerve stimulation and recording were attached to the skin connector (Fig. 2A and B). Arterial pressure was measured by telemetry. After carefully arranging the two electrodes and the delivery device, nerve stimulation with either distal or proximal nerve blockade was performed.

Nerve impulses were evoked by electrical stimulation of the vagus from the cuff electrode distal to the targeted delivery device (Fig. 3A). Rectangular pulses were delivered using a stimulator (SEN-7103, Nihon Kohden) and an isolator (SS-202J, Nihon Kohden). For in vivo electrophysiology, the stimulation frequency was 1 Hz and the pulse duration was 0.3 ms. The magnitude of stimulation was set at a supramaximal level (1.2–2.0 V). For functional experiments examining the AP and HR responses, the stimulation frequency, pulse duration, and magnitude were set at 10–30 Hz, 0.2–1 ms, and 2 V, respectively. The compound action potential (CAP) was amplified using an AC amplifier (200,000×, Model AB-610J, Nihon Kohden) with low (150 Hz) and high (1 kHz) frequency cutoffs. Nerve signals and arterial pressure data were sampled using a 12-bit A/D converter. Nerve signals were digitized at 5 kHz per electrode channel. The data were saved onto the hard disk of a dedicated laboratory computer system for later analysis.

2.4. Statistics

Data were reported as mean ± S.D. values. Changes in HR and MAP were compared before and during the stimulation by paired *t*-tests with the significance level set at $p < 0.05$.

3. Results

Fig. 3B shows the CAP of the vagus nerve evoked by electrical stimulation from the cuff electrode. The CAP consisted of one main component propagating at 0.9–2.1 m/s, as well as fast (>3 m/s) and slow (<0.9 m/s) components. All components of the CAP disappeared after an injection of a small amount (<20 μl) of 1% lidocaine (Fig. 3C). The fast component had almost recovered 15 min after the injection, followed by recovery of the main component in 40 min. The slow component required longer to recover.

The rats stayed quiet during the injection of anesthetics, with no changes in baseline HR and MAP. The HR and AP responses to electric stimulation differed after blockade of the afferent nerves, compared with before blockade. Prior to nerve blockade, electric stimulation of the right vagus nerve decreased HR abruptly, whereas it was associated with an increase in MAP, as shown in Fig. 4; HR decreased from 434 ± 8 to 246 ± 35 bpm ($p < 0.01$), whereas MAP increased from 99 ± 11 to 127 ± 14 mmHg ($p < 0.01$). However, after the blockade of afferent fibers, electrical stimulation of the nerve decreased HR without significant changes in MAP (HR 414 ± 4 bpm versus 266 ± 17 bpm, $p < 0.01$; MAP 106 ± 12 mmHg versus 103 ± 14 mmHg). The effects of vagal afferent blockade were

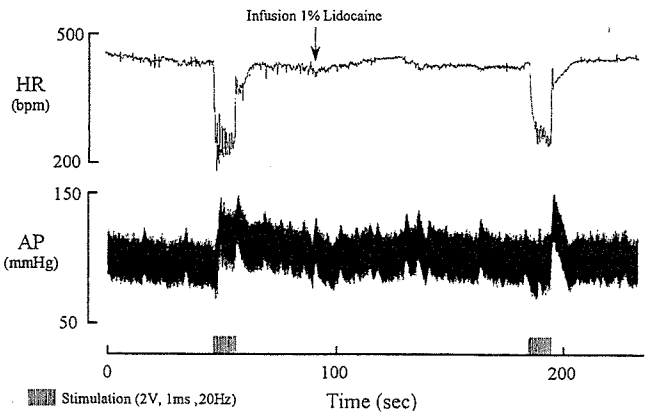

Fig. 4. Representative responses of arterial pressure (AP) and heart rate (HR) to electric stimulation (2 V, 1 ms, 20 Hz, 10 s) of the right vagus nerve before and after blockade of afferent fibers by local infusion of 1% lidocaine in conscious rats.

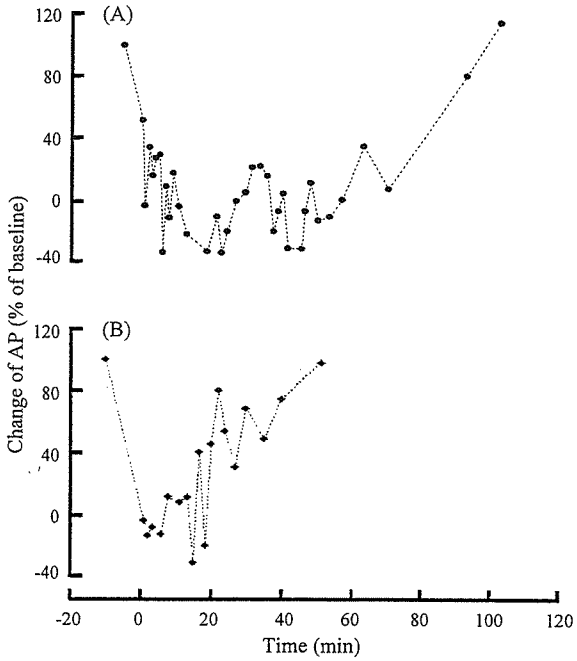

Fig. 5. Examples of the time course of the arterial pressure (AP) response to electric stimulation of cervical vagus nerve after afferent blockade by bolus infusion of 1% lidocaine in conscious rats. Each point represents the percentage of AP responses compared to the baseline response (before afferent blockade). Electric stimulations (2 V, 1 ms, 20 Hz, 10 s) were performed intermittently at interval greater than 1 min. The tests were done 1 week (A) and 2 weeks (B) after the implantation surgery.

reversible and the HR and MAP responses were restored in 15–60 min after the injection of 1% lidocaine. The duration of the nerve block was shorter in the second week than the first week (Fig. 5). The durability of the targeted delivery device was chiefly determined by how intact the infusion tube was. The effectiveness of the local blockade was confirmed 2 months after the implantation surgery.

4. Discussion

A variety of disease models, ranging from hypertension to heart failure, make the rat very important as an experimental animal for cardiovascular research. Reversible blockade of the autonomic nerves in small animals like the rat would be useful for physiological and behavioral study (Thalhammer et al., 1995), and would contribute to our understanding of the regulation of the cardiovascular system by the autonomic nervous system. We designed a targeted delivery device for the rat cervical vagus nerve. Using the targeted delivery device, in vivo electrophysiology and the functional evaluation of reversible nerve blockade were conducted in chronically instrumented, conscious rats. To our knowledge, this is the first study applying the targeted delivery device to blockade of the vagus nerve in conscious rats.

As shown in Fig. 3C, local injection of a small amount (<20 μl) of anesthetic (1% lidocaine) caused reversible, complete conduction block of the vagus nerve. The rats stayed calm in the rodent cage without any indication of significant stress during or after the injection of anesthetics. Temporary administration of anesthetics via the targeted delivery device lessens the stress compared to other techniques of nerve blockade requiring surgical procedures, and is therefore suitable for evaluating the role of the autonomic nervous system in circulatory regulation without significant sympathetic excitation associated with the stress. The infusion period and the type of anesthetics may control the duration of nerve blockade. For instance, lidocaine causes a relatively short-lived nerve blockade whereas marcaine causes a longer blockade. Selective anesthetics may also be used for vagal afferent blockade (Bowser-Riley et al., 1990). Fig. 5 shows that the duration of the nerve block lessoned over time after the implantation surgery even with the same dose of anesthetic. The space surrounding the nerve within the guide tube may be replaced by regenerated tissue over time after the surgical procedure, possibly reducing the effective volume of distribution for the anesthetic. Although vagal blockade has been reported to increase HR in large animals like ponies (Derksen et al., 1981), the vagal blockade did not increase baseline HR significantly in rats in the present study. The differences in the effects of vagal blockade on HR may be a result of species difference in basal vagal nerve activity.

The autonomic nerves usually contain both afferent and efferent fibers. Hence the selective stimulation or recording of either the afferent or efferent nerve is essential to assess the role of the autonomic nerves in circulatory regulation. Vagal afferent fibers conduct the signals from most of the organs in the thoracic and abdominal cavity to the medulla, stimulating various viscerogenic reflexes. Continuous electrical stimulation of the afferent fibers may exert intensity-dependent inhibition of breathing, anxiety, or even painful behavioral reactions, often accompanying the increase in arterial pressure. As shown in Fig. 4, prior to nerve blockade, right vagal stimulation decreased HR and increased MAP, and the increase in MAP was not observed after blocking the portion proximal to the stimulation electrodes, suggesting that the increase in MAP before the proximal blockade could be attributed to vagal afferent activation. Combining vagal afferent blockade with vagal stimulation, we were able to selectively evaluate the role of the vagal efferent function in conscious rats (Li et al., 2003).

In conclusion, we have demonstrated a reversible blockade of the vagus nerve in conscious rats. A complete conduction block was achieved by local administration of a minimal dose of anesthetics. The reversible nerve blockade can be combined with nerve stimulation or nerve recording techniques to stimulate or record the efferent or afferent autonomic nerve activity in conscious animals. This technique, involving the use of a targeted delivery device, has the potential to aid in furthering our understanding of the role of the autonomic nervous system in cardiovascular regulation, and to promote physiological and behavioral studies.

Acknowledgements

This study was supported by a "Health and Labour Sciences Research Grant for Research on Advanced Medical Technology" from the Ministry of Health, Labour and Welfare of Japan,

"Health and Labour Sciences Research Grant for Research on Medical Devices for Analyzing, Supporting and Substituting the Function of Human Body" from the Ministry of Health, Labour and Welfare of Japan, "Program for Promotion of Fundamental Studies in Health Science" from the National Institute of Biomedical Innovation, a Grant provided by the Ichiro Kanehara Foundation, "Ground-based Research Announcement for Space Utilization" promoted by Japan Space Forum, and "Industrial Technology Research Grant Program in 03A47075" from New Energy and Industrial Technology Development Organization (NEDO) of Japan.

References

Borgdorff P, Versteeg PG. An implantable nerve cooler for the exercising dog. Eur J Appl Physiol Occup Physiol 1984;53(2):175–9.

Bowser-Riley F, Cornish M, Kidd C, Zheng F. Role of vagal afferent C fibres in the bradycardiac response to an increase in arterial blood pressure in ferrets. Exp Physiol 1990;75(6):859–62.

Costanzo EM, Barry JA, Ribchester RR. Co-regulation of synaptic efficacy at stable polyneuronally innervated neuromuscular junctions in reinnervated rat muscle. J Physiol 1999;521(Pt 2):365–74.

Cudd TA. Vagal blockade does not prevent adrenocorticotropin, cortisol, and cardiopulmonary responses to thromboxane A2. Can J Physiol Pharmacol 1998;76(12):1087–94.

Derksen FJ, Robinson NE, Stick JA. Technique for reversible vagal blockade in the standing conscious pony. Am J Vet Res 1981;42(3):523–5.

Gokin AP, Philip B, Strichartz GR. Preferential block of small myelinated sensory and motor fibers by lidocaine: in vivo electrophysiology in the rat sciatic nerve. Anesthesiology 2001;95(6):1441–54.

Kanje M, Lundborg G, Edstrom A. A new method for studies of the effects of locally applied drugs on peripheral nerve regeneration in vivo. Brain Res 1988;439(1–2):116–21.

Lee LY, Morton RF, Kou YR. Acute effects of cigarette smoke on breathing in rats: vagal and nonvagal mechanisms. J Appl Physiol 1990;68(3):955–61.

Li M, Zheng C, Kawada T, Sato T. Vagal stimulation improved acute-phase survival after myocardial infarction in conscious rats. Circulation 2003;108(Suppl. IV):IV-268, 1268.

Potocnik I, Tomsic M, Bajrovic F. Sensitivity of sensory axons to lidocaine nerve block in rats. Pflugers Arch 2001;442(6 Suppl. 1):R193–4.

Schultz HD, Gardner DG, Deschepper CF, Coleridge HM, Coleridge JC. Vagal C-fiber blockade abolishes sympathetic inhibition by atrial natriuretic factor. Am J Physiol 1988;255(1 Pt 2):R6–13.

Thalhammer JG, Vladimirova M, Bershadsky B, Strichartz GR. Neurologic evaluation of the rat during sciatic nerve block with lidocaine. Anesthesiology 1995;82(4):1013–25.

Vizek M, Frydrychova M, Houstek S, Palecek F. Effect of vagal cooling on lung functional residual capacity in rats with pneumonia. Bull Eur Physiopathol Respir 1983;19(1):23–6.

Am J Physiol Heart Circ Physiol 291: H318–H326, 2006.
First published February 24, 2006; doi:10.1152/ajpheart.00975.2005.

Short-term electroacupuncture at Zusanli resets the arterial baroreflex neural arc toward lower sympathetic nerve activity

Daisaku Michikami,[1,2] Atsunori Kamiya,[1] Toru Kawada,[1] Masashi Inagaki,[1] Toshiaki Shishido,[1] Kenta Yamamoto,[1,2] Hideto Ariumi,[1,2] Satoshi Iwase,[3] Junichi Sugenoya,[3] Kenji Sunagawa,[4] and Masaru Sugimachi[1]

[1]Department of Cardiovascular Dynamics, Advanced Medical Engineering Center, National Cardiovascular Center Research Institute, Osaka; [2]Pharmaceuticals and Medical Devices Agency, Tokyo; [3]Department of Physiology, School of Medicine Aichi Medical University, Nagakute, Aichi; and [4]Department of Cardiovascular Medicine, Kyushu University Graduate School of Medical Sciences, Fukuoka, Japan

Submitted 12 September 2005; accepted in final form 17 February 2006

Michikami, Daisaku, Atsunori Kamiya, Toru Kawada, Masashi Inagaki, Toshiaki Shishido, Kenta Yamamoto, Hideto Ariumi, Satoshi Iwase, Junichi Sugenoya, Kenji Sunagawa, and Masaru Sugimachi. Short-term electroacupuncture at Zusanli resets the arterial baroreflex neural arc toward lower sympathetic nerve activity. *Am J Physiol Heart Circ Physiol* 291: H318–H326, 2006. First published February 24, 2006; doi:10.1152/ajpheart.00975.2005.—Although electroacupuncture reduces sympathetic nerve activity (SNA) and arterial pressure (AP), the effects of electroacupuncture on the arterial baroreflex remain to be systematically analyzed. We investigated the effects of electroacupuncture of Zusanli on the arterial baroreflex using an equilibrium diagram comprised of neural and peripheral arcs. In anesthetized, vagotomized, and aortic-denervated rabbits, we isolated carotid sinuses and changed intra-carotid sinus pressure (CSP) from 40 to 160 mmHg in increments of 20 mmHg/min while recording cardiac SNA and AP. Electroacupuncture of Zusanli was applied with a pulse duration of 5 ms and a frequency of 1 Hz. An electric current 10 times the minimal threshold current required for visible muscle twitches was used and was determined to be 4.8 ± 0.3 mA. Electroacupuncture for 8 min decreased SNA and AP (n = 6). It shifted the neural arc (i.e., CSP-SNA relationship) to lower SNA but did not affect the peripheral arc (i.e., SNA-AP relationship) (n = 8). SNA and AP at the closed-loop operating point, determined by the intersection of the neural and peripheral arcs, decreased from 100 ± 4 to 80 ± 9 arbitrary units and from 108 ± 9 to 99 ± 8 mmHg (each $P < 0.005$), respectively. Peroneal denervation eliminated the shift of neural arc by electroacupuncture (n = 6). Decreasing the pulse duration to <2.5 ms eliminated the effects of SNA and AP reduction. In conclusion, short-term electroacupuncture resets the neural arc to lower SNA, which moves the operating point toward lower AP and SNA under baroreflex closed-loop conditions.

arterial pressure; equilibrium diagram

ALTHOUGH THERE ARE MANY clinical case reports (21, 30, 32, 39, 40, 42), the effects of electroacupuncture on cardiovascular regulation remain to be systematically investigated. There has been a recent renewal of interest in the inhibitory effects of electroacupuncture of the Zusanli acupoint on the cardiovascular system, including reductions in arterial pressure (AP), heart rate, (3, 15, 16), and sympathetic nerve activity (SNA) (25, 42). Such inhibitory effects are observed during low-frequency (<20 Hz) electroacupuncture. Because the arterial baroreflex is one of the most important control systems that stabilize AP, we quantified the effects of electroacupuncture on the arterial baroreflex over an entire operating range. Systematic analysis would help to assess the possible utility of electroacupuncture as a treatment modality for certain cardiovascular diseases with vagolytic and sympathotonic states (26, 38).

One of the best ways to quantitatively analyze changes in the arterial baroreflex over an entire operating range may be analysis using a baroreflex equilibrium diagram (10, 23, 31) (see APPENDIX for details). Briefly, the baroreflex equilibrium diagram consists of a neural arc representing SNA as a function of baroreceptor input pressure and a peripheral arc representing AP as a function of SNA. The intersection of the two arcs corresponds to an operating point of the AP regulation under baroreflex closed-loop conditions. Considering the reduced AP and SNA found in previous studies, we hypothesized that short-term electroacupuncture resets the arterial baroreflex neural arc to lower SNA. In the present study, to test this hypothesis, we constructed a baroreflex equilibrium diagram with neural and peripheral arcs in anesthetized rabbits. The present findings indicate that electroacupuncture resets the baroreflex neural arc to lower SNA, moving the closed-loop operating point toward lower AP and SNA.

MATERIALS AND METHODS

Surgical Preparation

Animals were cared for in strict accordance with the *Guiding Principles for the Care and Use of Animals in the Field of Physiological Sciences* approved by the Physiological Society of Japan. Twenty-two Japanese White rabbits weighing 2.4–3.3 kg were anesthetized via intravenous injection (2 ml/kg) with a mixture of urethane (250 mg/ml) and α-chloralose (40 mg/ml) and mechanically ventilated with oxygen-enriched room air. Supplemental doses were injected as necessary (0.5 ml/kg) to maintain an appropriate level of anesthesia. Body temperature was maintained at ~38°C with a heating pad. AP was measured by using a high-fidelity pressure transducer (SPC-330A, Millar Instruments, Houston, TX) inserted via the left femoral artery. To record cardiac SNA, we exposed the left cardiac sympathetic nerve through a midline thoracotomy and attached a pair of stainless steel wire electrodes (Bioflex wire AS633, Cooner Wire, Chatsworth, CA) to the nerve. The nerve fibers peripheral to the

Address for reprint requests and other correspondence: D. Michikami, Dept. of Cardiovascular Dynamics, Advanced Medical Engineering Center, National Cardiovascular Center Research Institute, 5-7-1 Fujishirodai, Suita, Osaka 565–8565, Japan (e-mail: dmichi@ri.ncvc.go.jp or kamiya@ri.ncyc.go.jp).

The costs of publication of this article were defrayed in part by the payment of page charges. The article must therefore be hereby marked "*advertisement*" in accordance with 18 U.S.C. Section 1734 solely to indicate this fact.